

Nanoscale

Accepted Manuscript



This is an *Accepted Manuscript*, which has been through the Royal Society of Chemistry peer review process and has been accepted for publication.

Accepted Manuscripts are published online shortly after acceptance, before technical editing, formatting and proof reading. Using this free service, authors can make their results available to the community, in citable form, before we publish the edited article. We will replace this *Accepted Manuscript* with the edited and formatted *Advance Article* as soon as it is available.

You can find more information about *Accepted Manuscripts* in the [Information for Authors](#).

Please note that technical editing may introduce minor changes to the text and/or graphics, which may alter content. The journal's standard [Terms & Conditions](#) and the [Ethical guidelines](#) still apply. In no event shall the Royal Society of Chemistry be held responsible for any errors or omissions in this *Accepted Manuscript* or any consequences arising from the use of any information it contains.



The functional dissection of the plasma corona of SiO₂-NPs spots Histidine Rich Glycoprotein as a major player able to hamper nanoparticles capture by macrophages

Received 00th 20xx,
Accepted 00th 20xx

DOI: 10.1039/x0xx00000x

www.rsc.org/

Chiara Fedeli,^{a,b} Daniela Segat,^{c,†} Regina Tavano,^{a,b} Luigi Bubacco,^c Giorgia De Franceschi,^a Patrizia Polverino de Laureto,^a Elisa Lubian,^d Francesco Selvestrel,^d Fabrizio Mancin^{d*} and Emanuele Papini^{a,b*}

A coat of strongly-bound host proteins, or *hard corona*, may influence the biological and pharmacological features of nanotheranostics by altering their cell-interaction selectivity and macrophages clearance. With the goal of identifying specific corona-effectors, we investigated how the capture of amorphous silica nanoparticles (SiO₂-NPs; $\emptyset = 26$ nm; zeta potential = -18.3 mV) by human lymphocytes, monocytes and macrophages is modulated by the prominent proteins of their plasma corona. LC MS/MS analysis, western blot and quantitative SDS-PAGE densitometry show that Histidine Rich Glycoprotein (HRG) is the most abundant component of the SiO₂-NPs hard corona in excess plasma from humans (HP) and mice (MP), together with minor amounts of the homologous Kininogen-1 (Kin-1), while it is remarkably absent in their Foetal Calf Serum (FCS)-derived corona. HRG binds with high affinity to SiO₂-NPs (HRG K_d ~2 nM) and competes with other plasma proteins for the NPs surface, so forming a stable and quite homogeneous corona inhibiting nanoparticles binding to the macrophage membrane and their subsequent uptake. Conversely, in the case of lymphocytes and monocytes not only HRG but also several common plasma proteins can interchange in this inhibitory activity. The depletion of HRG and Kin-1 from HP or their plasma exhaustion by increasing NPs concentration (>40 μ g/ml in 10% HP) lead to a heterogeneous hard corona, mostly formed by fibrinogen (Fibr), HDLs, LDLs, IgGs, Kallikrein and several minor components, allowing nanoparticle binding to macrophages. Consistently, the FCS-derived SiO₂-NPs hard corona, mainly formed by hemoglobin, α 2 macroglobulin and HDLs but lacking HRG, permits nanoparticles uptake by macrophages. Moreover, purified HRG competes with FCS proteins for the NPs surface, inhibiting their recruitment in the corona and blocking NPs macrophage capture. HRG, the main component of the plasma-derived SiO₂-NPs *hard corona*, has antiopsonine characteristics and uniquely confers to these particles the ability to evade macrophages capture.

Introduction

The success of the huge effort devoted to design effective nanoparticles (NPs) for therapy and diagnosis strongly needs parallel investigations on the interactions of such systems with biological media. Indeed, only by understanding the interplay between nanoparticles and biological entities it will be possible to rationally plan the desired action mechanism of

nanotheranostics. It is now well established that the surface of the nanoparticle is a crucial variable determining such interactions and consequently the nanoparticle's biological effects. On the other hand, it is also quite clear that the first event occurring to the nanoparticle, once entered in a biological environment, is the formation of a surface adsorbed layer of proteins, named *protein corona*.¹⁻¹⁵ The protein corona formation *in vivo* is likely a major actor at the host/nanoparticle interface, deeply influencing the bioactivity and the bioavailability of nanosystems.¹⁶ Available evidence suggests that the protein corona composition varies depending on several factors including the nanoparticle material, surface functionalization, size, shape and biological environment. Although relatively small subsets of the many proteins available in biological fluids are normally found to bind nanoparticles, still the reported corona compositions involve from tens to few hundreds of polypeptides. Simple geometric considerations make however difficult to rationalize, especially for small nanoparticles (< 30 nm diameter), the physical co-existence in the same corona of hundreds of different protein

^a Centro di Ricerca Interdipartimentale per le Biotecnologie Innovative, Università di Padova, via U. Bassi 58/B, I-35131, Padova, Italy.

^b Dipartimento di Scienze Biomediche, Università di Padova, via U. Bassi 58/B, I-35131, Padova, Italy.

^c Dipartimento di Biologia, Università di Padova, via U. Bassi 58/B, I-35131, Padova, Italy

^d Dipartimento di Scienze Chimiche, Università di Padova, via Marzolo 1, I-35131 Padova, Italy

[†] Current address: Institute for Rare Diseases 'Mauro Baschirotto', via B. Bizio 1, 36023 Costozza di Longare (Vicenza), Italy.

Electronic Supplementary Information (ESI) available: Additional uptake and corona characterization experiments, proteins purifications, DLS experiments, proteins affinity and geometrical calculations, protein tables. See DOI: 10.1039/x0xx00000x

types, in particular when one considers that some of them have a size comparable to or even larger than the NP itself. Indeed, semi-quantitative estimations by label-free methods after shotgun LC MS/MS analysis show that, beside few main corona components, expected to cover the major part of the NPs surface, the majority of the other polypeptides found associated to the NPs are indeed present in substoichiometric ratios (< 1 polypeptide per nanoparticle).¹²⁻¹⁴ This observation somehow resolves the paradox of accommodating too many components in the same corona, but introduces an additional level of heterogeneity of the corona-coated NPs, because it implies the presence of several subsets of nanoparticles each characterized by its own corona, with fewer polypeptides but with specific composition differences. Additional complexity is provided by the fact that the first shell of strongly bound proteins (hard corona) can reversibly interact with other proteins forming the so called *soft corona* and enlarging the number of proteins coating the nanoparticle.¹⁷

The above considerations may suggest that the goal of fully understanding the nanoparticle corona functional complexity, with the aim to predict the biocompatibility and pharmacological properties of a candidate nanosystem, may be a too demanding task. On the other hand, recent statistical and correlative studies with gold NPs indicate that small subsets of the corona polypeptides (6-10 out of the ~ 400 found) may be the major functional actors influencing the nanoparticle biological characteristics, so that focused detection of their presence in the corona has been proposed as a useful tool to predict nanoparticles efficacy to enter cells.⁵ Therefore, the functional discrimination of the corona components that *play the lead roles* from *background actors*, and the definition of the nanoparticle surface features controlling their selection, may become mandatory information for the design of efficient theranostic nanosystems. To achieve this goal, the individuation of simplified models for corona investigations and the calibration of suitable experimental conditions and test candidates capable to provide really predictive data are of paramount importance.¹⁸

In this paper we focus our attention on silica nanoparticles (SiO₂-NP), which are attracting a great attention as potential nanomedicine candidates¹⁹ and on monocytes and macrophages phagocytic cells of the reticular endothelial system (RES)/mononuclear phagocyte system (MPS). Indeed, these cells are especially exposed to nanoparticles after blood injection, due to their particulate capturing specialization, and represent a good starting point to understand the interaction of nanoparticles with biological entities and how the protein corona can affect the nanoparticles properties. It may be expected that nanoparticles efficiently internalized by such cells will be rapidly removed by circulation in vivo and accumulated in the main filtering organs, as liver and spleen. On the contrary, nanoparticles capable to escape phagocytic capture will circulate longer and may eventually reach different tissues. The central role of RES/MPS clearance in determining the efficacy of nanotheranostics have been recently highlighted in mice models and humans.²⁰

One of the acknowledged effect of protein corona is the reduction of nanoparticles uptake by many cell types.^{21, 22} We have previously reported that such protection activity is present in the case of lymphocytes, used as representative of cells without phagocytic activity, and in monocytes, when incubated with 30 nm-diameter SiO₂-NPs in the presence of Foetal Calf Serum (FCS), but is remarkably not working in macrophages.^{23, 24} With these cells, SiO₂-NPs capture in FCS is very high and comparable to that observed in protein free media. Such a behaviour has been reported also for other nanomaterials in similar conditions.²⁵ However, extrapolation to the human context is dubious²⁶ especially because proteomic analysis clearly indicates that nanoparticle protein hard-corona formed in FCS is distinctively different from that formed in human plasma (HP).^{21, 27} Moreover coagulation and complement components, immunoglobulins (IgG) and lipoproteins are defective in FCS compared to HP.²⁸

In this view, we explored and compared the composition of the coronas formed on SiO₂-NPs upon incubation with different protein sources, *i.e.* the commonly used Foetal Calf Serum (FCS), mouse plasma (MP) and human plasma (HP). In doing this, we paid close attention to the effect of the nanoparticle *dose* in influencing the corona composition. Eventually, we ascertained the role of the single major proteins composing the corona formed in HP in determining the interaction of the nanoparticles with phagocytic or non-phagocytic cells. Interesting and stimulating results emerged from this investigation: i) the hard-corona formed in HP strongly changes the cell binding selectivity of SiO₂-NPs compared to the FCS-derived hard-corona; ii) a single protein, namely Histidine Rich Glycoprotein (HRG) emerges as the main component of the HP/MP-derived SiO₂-NPs hard-corona, but not of the FCS-derived one, and is responsible for the different behaviour of the nanoparticles in the two biofluids; iii) HRG uniquely confers to SiO₂-NPs the ability to reduce macrophages capture in vitro, a specific stealthing property missing to other major human plasma proteins.

Results

Differential effect of FCS and HP on SiO₂-NPs macrophage binding.

To get more insight on the role played by plasma protein corona in cell interactions, we prepared fluorescein-labelled 26 nm-diameter silica nanoparticles, produced by the Stöber-Van Blaaderen protocol,²⁹⁻³¹ and analysed their uptake by HepG2, a cell line from human hepatocarcinoma, primary human lymphocytes, monocytes and macrophages in the absence of protein and in the presence of FCS and HP (both 10% v/v). Low nanoparticles doses (< 40 µg/ml) were used both to avoid potential confounding factors arising from cytotoxic and proinflammatory effects and to better simulate the high dilution condition presumably experienced by nanoparticles after injection in the bloodstream. The results obtained are very interesting (Figure 1). In agreement with previous observations, cell capture of SiO₂-NPs, after 3 hours in

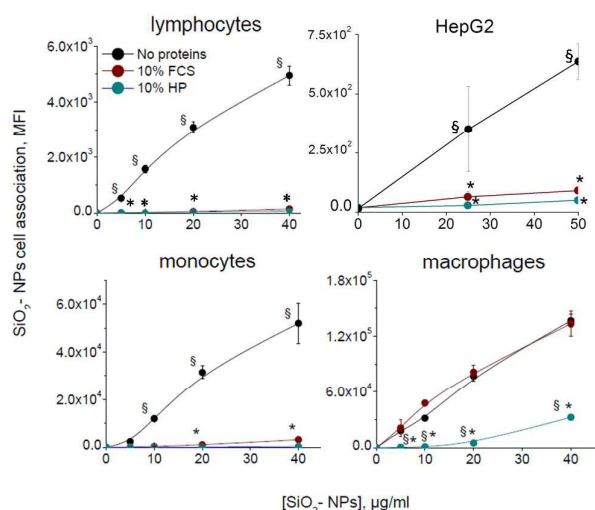


Figure 1. Comparison of the effects of FCS and HP on the binding of SiO₂-NPs to lymphocytes, HepG2, monocytes and macrophage. Indicated cells were incubated in RPMI 1640 medium without proteins (no proteins), plus 10% (v/v) FCS or 10% (v/v) HP, as indicated, for 3h at 37°C with SiO₂-NPs at the indicated concentrations, and analysed by flow cytometry. Data, expressed as Mean Fluorescence Intensity, were acquired keeping the same instrument settings to ensure comparison. Note that Y axis scales are different in the four cells. Values are the means from experiments run in duplicate \pm SE (N=4). * significance ($p < 0.05$) with respect to no protein; § significance ($p < 0.05$) with respect to FCS.

protein-free media is strongly inhibited by FCS in HepG2, lymphocytes and monocytes (> 80%, > 99%, > 95% inhibition respectively) while not affected in macrophages.^{23, 24} The behaviour observed in human plasma (HP) is substantially different. Indeed, incubation in this medium results in an increased inhibition of SiO₂-NPs uptake by HepG2 cells, lymphocytes and monocytes and, at difference from FCS, also by macrophages (~90-95% inhibition). This protective effect of HP is particularly efficient at low particle doses (< 20 µg/ml) and is still observed after prolonged incubation times in the same conditions up to 20 h (Figure S1).

Characterization of the SiO₂-NPs corona composition in FCS and in human and mouse plasma.

A reasonable hypothesis to explain the observed difference between HP and FCS in affecting SiO₂-NPs macrophage uptake is that one or more proteins selectively present in the HP-derived NPs corona, while not in the FCS-derived one, can hamper the special ability of macrophages to engage NPs. Therefore, we analysed the protein corona formed on nanoparticles incubated for 15 minutes at 37°C in the two media. After NPs recovery and extensive washing by ultracentrifugation, associated proteins were subjected to gradient gel electrophoresis in non-reducing conditions, evidenced by the very sensitive silver staining and eventually analysed by densitometry (Figure 2).

Both the apparent molecular weight and the intensity of the major bands, in agreement with other studies,^{18,25} confirm that the pattern of the main proteins strongly associated to NPs varies considerably depending on the protein medium.

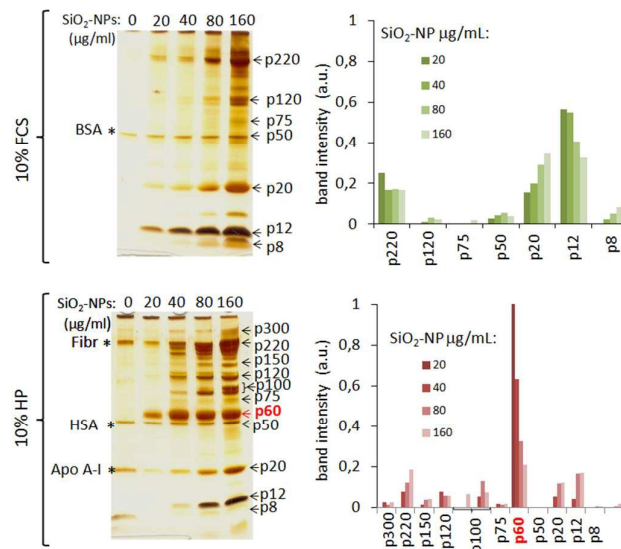


Figure 2. SDS-PAGE analysis the pattern of FCS and HP proteins adsorbed on SiO₂-NPs. SiO₂-NPs were incubated at the indicated concentrations for 15 minutes at 37°C in RPMI 1640 plus 10% FCS or 10% HP, as specified, isolated and subjected to 4-20% gradient SDS-PAGE (left). Equal samples volumes and so increasing NPs amounts per lane were loaded. After Silver staining, a semi-quantitative estimation of the relative amount of the main protein bands found (arrows), labelled by their rough apparent molecular weight in KDa (pxx), were determined by densitometry and represented in histograms (right). The intensity of each band was normalized over the sum of the intensities of all the bands within the same lane. * indicate the major background proteins present in the samples treated without NPs (mock samples) and recovered from FCS (BSA) and HP (Fibr, HSA, Apo A-I). Gels are from representative experiments out of four.

Moreover, the protein pattern also varies with the nanoparticles concentration, particularly in the case of HP. In this medium a peculiar observation is that, at NPs concentrations below 40 µg/ml, a single protein band with an apparent MW of 60 KDa (p60) predominates in the pattern, while above this dose (NPs 80-160 µg/ml) several other protein bands, either with higher or with lower molecular weights become also evident. The main bands observed (7 for FCS and 12 for HP) were then analysed by LC MS/MS to obtain a semi-quantitative evaluation of their polypeptide composition and relative proportion, using well-established bioinformatics label-free parameters.³² In 10% FCS (Figure 3A, Table S1 for detailed MS analysis), the major electrophoretic bands corresponded to haemoglobin (p12), α 2-macroglobuline (p220) and HDL-associated Apo A-I (p20). Other constituents are HDL-associated Apo A-II (p8), albumin (p50), complement Factor H (Fh) (p120) and plasminogen (PLG) (p75).

A remarkably different pattern was found with 20 µg/ml SiO₂-NPs in 10% HP (Figure 3B, Table S2 for detailed MS analysis). Here, based on emPAI label free evaluation, using a cut of > 1 significant peptides identified,³³ the most stained band (p60) was found to be essentially made by HRG (70% HRG, 11% Kin-1) while the second less intense one (p100) was mostly formed by Kin-1 (76% Kin-1 and 13% HRG). At the NPs concentration of 160 µg/ml the p60 band was still present and was again formed by HRG (HRG 86%, Vitronectin 14%) but within the

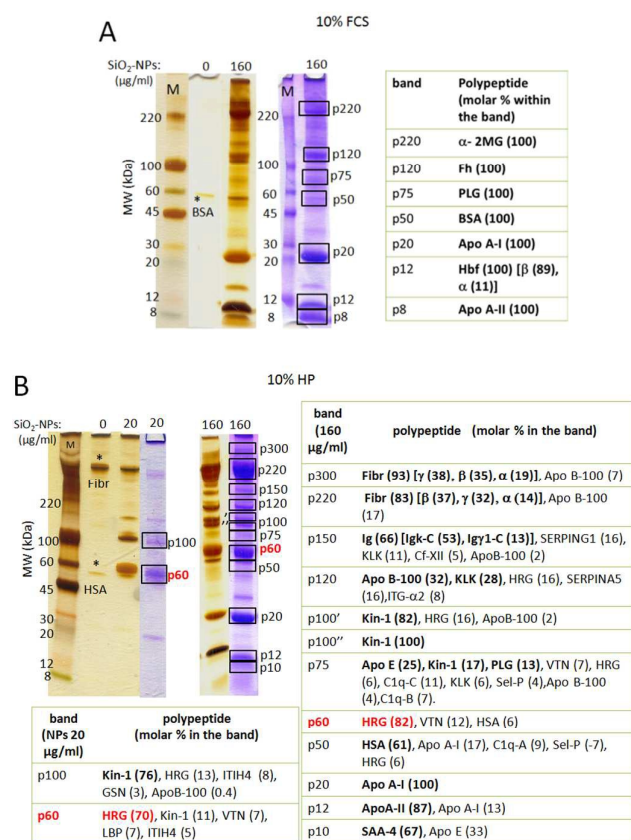


Figure 3. Characterization of the pattern of FCS and HP polypeptides adsorbed on SiO₂-NPs by LC MS/MS. The SDS-PAGE bands, in yellow boxes, corresponding to the major corona proteins formed on SiO₂-NPs after incubation for 15' at 37°C with RPMI plus 10% FCS (A) or 10% HP (B) at the indicated nanoparticle concentrations, were excised from Coomassie stained gel and analysed by LC MS/MS to identify their protein composition (see Materials and Methods for details). Silver stained samples are shown in parallel for comparison. Positive hits (polypeptide with at least 2 significant matches, $p < 0.05$) are listed in the table, with their molar % within the same band, based on empAI, reported in brackets. Main proteins are indicated in bold; asterisks indicate non-specific bands from FCS and HP mock controls (no NPs). M: standard molecular weight. Abbreviation used: α -2MG: alpha-2 macroglobulin; Apo A-I/A-II/B-100/E: apolipoprotein A-I/A-II/B-100/E; BSA: bovine serum albumin; CF-XII: coagulation factor XII; C1q-A,B,C: complement C1q subunit A,B,C; Fh: complement factor H; Fibr: fibrinogen; GSN: gelsolin; Hbf α/β : foetal haemoglobin; HRG: histidine rich glycoprotein; Ig: immunoglobulins; ITG- α 2: integrin alpha; ITIH4: Inter-alpha-trypsin inhibitor heavy chain H4; Kin-1: kininogen-1; KLK: Kallikrein; LBP: lipopolysaccharide-binding protein; PLG: plasminogen; SAA-4: serum amyloid A-4 protein; Sel-P: selenoprotein-P; SERPINA5: plasma serine protease inhibitor; SERPING1: plasma protease C1 inhibitor; VTN: vitronectin.

context of a more complex set of bands. Focusing on major components, it can be noted that: the p300 band is formed by Fibr (93%) and by the LDL marker Apo B-100 (7%) similarly to p220 (Fibr 83% Apo B-100 17%); p150 is a mixture of IgG (66%), SERPING1 (16%) and KLK (11%); p120 is more heterogeneous (32% Apo B-100 fragment, 28% Kallikrein, 16% HRG and 16% plasma serine protease C1 inhibitor; the two close bands p100'/p100'' both corresponded to Kin-1 (Kin-1 91%, HRG 8%); the faint p75 band was heterogeneous (25% Apo E, 17% Kin-1, 13% PLG). Band p50 was made principally by HSA (61%) and by a mixture of other minor protein being

Apo A-I the most relevant (17%). However, it is important to note that this band seems present with similar intensity also in the mock NPs free sample, indicating that it may be a remnant from plasma. Band p20 is ~100% formed by the HDL marker Apo A-I, while p12 is mostly Apo A-II (87%, Apo A-I 13%) and p10 is made by SAA-4 67% plus a fragment of the LDL maker Apo E (26%).

After correction of empAI for sample loading, which varied for different bands to ensure sufficient counts for the faintest bands, and correction for quaternary structures, when necessary, we could obtain an estimation of the relative molar content of found proteins associated to the NPs (Figure S2A, B). Results are in good agreement with densitometry estimation and indicate that at low NPs doses HRG and Kin-1 are the major proteins accounting for more than 90% of the total proteins. Again in agreement with densitometry, HRG and Kin-1 are still present at 160 µg/ml, about 10% of total proteins each, but several other proteins are now detected. Among these the most prevalent are Ig (8%), Fibr (14%), LDL (16%) (using Apo B-100 and Apo E as bona fide markers) and HDL (18%) (using Apo A-I and Apo A-II as bona fide markers). The amounts of the major polypeptides forming the HP-derived protein coronas do not change grossly by increasing the incubation time of the nanoparticles up to 6 hours (Figure S3), indicating that the composition observed represents the kinetically stable state (hard corona) in the experimental conditions.

Since in other studies the protein corona forming around SiO₂ and other NPs was analysed after incubation at 0-4°C and in the presence of higher HP concentrations,^{11, 34} we tested the prevalence of HRG also in these conditions (Figure S4, Figure S5A and Table S3). After subtraction of plasma background, mock run in the absence of NPs (some of the proteins found in the NPs samples were indeed totally – Fibr and HSA – or in part – Ig and Apo A-I/HDL – due to background from plasma) and band analysis by LC MS/MS we confirmed that even in the more physiological conditions of ~100% HP, a major band made prevalently by HRG is still predominant both at 37°C and 4°C. However, Kin-1 tended to decrease compared to the amount found in 10% HP while minor amounts of the IgG isotypes, F-XI and other polypeptides are identified in samples (Table S3).

In other controls we also compared our NPs-corona isolation and washing procedure with the one recently developed by Tenzer *et al.*,¹² involving a direct layering of the NPs after incubation with HP on a sucrose cushion to ensure effective separation from unbound plasma proteins. Even with this procedure, the pattern of the protein specifically associated to the NPs corona at both 10% and 100% HP was still largely characterized by the presence of HRG as the major constituent at both 37°C and 4°C (see supplementary methods and Figure S4).

A similar composition, characterized by the prevalence of HRG, was also found after incubation of the nanoparticles with mouse plasma. In this medium, there are two peculiarities compared to HP: the additional presence of high level of haemoglobin, due to the higher haemolysis characterizing the

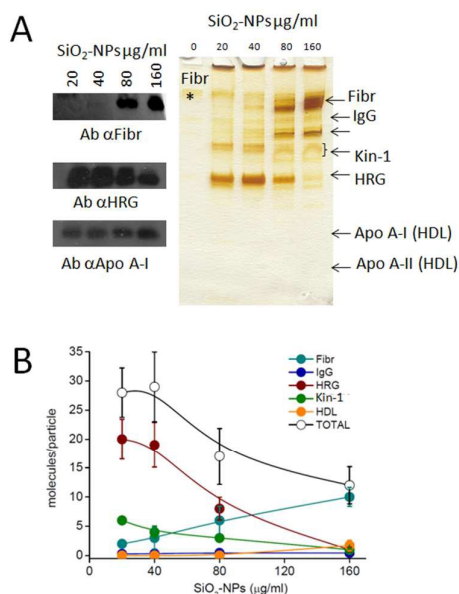


Figure 4. Absolute quantification of the main protein composing the HP-derived hard corona of SiO₂-NPs as a function of nanoparticles concentration. A) Representative SDS-PAGE analysis, out of five, showing the changes of the pattern of the major proteins bound to SiO₂-NPs (same quantity of NPs (13 μg)/lane), as a function of nanoparticle concentration during incubation for 15 min in 10% HP at 37°C. Differently than in gels of figure 2, where increasing amounts of NPs were analysed, here decreasing sample volumes were loaded per lane to ensure the comparison of equal NPs quantities (13 μg/lane). The presence of Fibrinogen, Histidine Rich Glycoprotein and Apo A-I was confirmed by Western Blot analysis using specific antibodies (left panels). B) The amounts of the main human plasma protein molecules per particle unit were calculated, after densitometry of the corresponding bands and comparison with titration curves made in parallel in the same SDS-PAGE gel with purified human protein standards (see Fig. S6A and relative legend). The obtained molecular composition of the hard-corona is reported as a function of NPs concentration; values are means ± SE (N=5). Lines have been depicted to guide the eye.

sampling of this fluid and, more interesting, the still high prevalence of HRG even at high NPs concentration, suggesting the presence of an higher level of this protein in MP (Figure S2B, Figure S5B, Table S4).

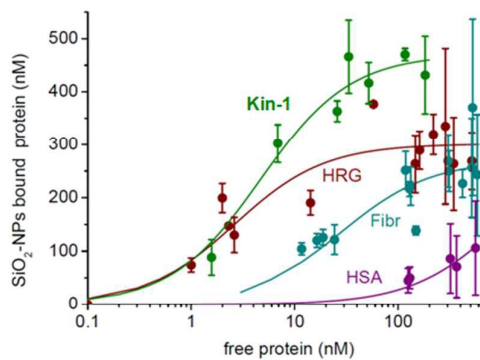
Having identified the major proteins of the SiO₂-NPs corona we performed a quantitative SDS-PAGE analysis to determine with an independent methodology their absolute amount per particle. This was achieved by calibrating the staining intensity of the most prominent bands, using standard purified proteins corresponding to their major components based on label-free MS analysis, after loading the same known amount of NPs per lane. Data confirmed the above described picture and provide other consistent information (Figure 4, Figure S6). In fact, the major ~ 60 kDa and ~ 220 kDa bands identified as principally formed by HRG and Fibr, were indeed found to have the same electrophoretic mobility as purified human HRG and Fibr. This further supports that indeed these two proteins forms the bulk of these two bands, as suggested by label-free methods. Again in agreement with label-free quantifications, this quantification also showed that Kin-1 is the second major component of the hard corona at low NPs concentration besides HRG (although in smaller proportion: HRG:Kin-1 ratio =

2.9 by quantitative densitometry, while 1.4 using emPAI). Also in this analysis, as the nanoparticles amount increased, HRG and Kin-1 sensibly decreased while Fibr and other proteins increased. More in detail, we could determine that below 40 μg/ml concentration a single NP has a corona formed by about 19-20 HRG, 5-7 Kin-1, and 2-3 Fibr molecules (sum: 26-30 molecules). These numbers change to 8 HRG, 3 Kin-1 and 6 Fibr (sum: 17 molecules) at 80 μg/ml NPs and to about 1 HRG, 1 Kin-1 and 10 Fibr (sum: 12 molecules) at 160 μg/ml NPs. Such figures allow estimating footprints values of about 50 nm² for HRG (64 kDa) and Kin-1 (70 kDa) and 170 nm² for Fibr (340 kDa), which are in good agreement with the proteins' molecular weights and hydrodynamic diameters (see *infra*). This peculiar switch in the protein corona from a HRG-rich composition to a Fibr-rich one, depending on the NPs dose (in 10% HP) was validated by western blot analysis using specific antibodies. Once again HRG signal decreased with NPs increase, while HDL (Apo A-I) and, much strongly, Fibr increased above 40 mg/ml NPs.

In summary, considering the three independent evidence collected, at low NPs doses, which better simulate the situation occurring *in vivo*, HRG and Kin-1 appear the most represented proteins on NPs, forming a coat of about 30 proteins with a molar ratio around 3:1. The concentrations of these two proteins in the culture media are relatively low, namely 15 and 8 μg/ml respectively for HRG and Kin-1. It is hence expected that when these first two proteins are depleted from the solution by increasing the NPs dose, they undergo surface-dilution leaving space available for the recruitment of other proteins, in particular Fibrinogen.

Affinity of HRG and other major plasma proteins for SiO₂-NPs.

The above data indicate that, in conditions of nanoparticle surface limitation (NPs concentration < 40 μg/ml), HRG and Kin-1 (~15 and ~8 μg/ml in 10% HP, respectively) prevent the binding of more concentrated protein like HSA (~5-6 mg/ml in 10% HP), Fibr (~300 μg/ml in 10% HP), and IgG (~700 μg/ml in 10% HP). This indicates that HRG and Kin-1 should have a significantly higher affinity for the negatively charged silica surface than other plasma proteins. Such a prediction was confirmed by measuring the affinity of purified HRG, Kin-1, fibrinogen and HSA for SiO₂-NPs. Experiments were performed by measuring the amount of residual free protein at equilibrium after elimination of the particle-protein complexes by ultracentrifugation and fitting the bound versus free protein data with the one site equilibrium equation (see methods) (Figure 5). We found that the dissociation constant (K_d) of the HRG-NPs complex was 2.4 ± 1.1 nM and that the maximal binding capability of a single particle was 30 ± 2 molecules per particle, a value in very good agreement with that obtained by gel quantification in HP. As expected, Kin-1 affinity was similar to that of HRG (4.6 ± 1.3 nM) while that of Fibr and in particular of HSA, where smaller (28 nM \pm 12 and > 1 μM respectively). Notably, in agreement with our data, two recent studies^{35,36} show that relatively high K_d values (37 ± 12 μM and 0,3-6 μM respectively) characterise the binding of HSA to variously modified negatively charged QDs.



Protein	K _d (nM)	B _{max} (mol/par)
HRG	2.4 ± 1.1	30 ± 2
Kin-1	4.6 ± 1.3	47 ± 2
Fibr	28 ± 12	27 ± 3
HSA	> 1000	n.d.

Figure 5. Estimation of the affinity of HRG, Kin-1, Fibr and HSA for SiO₂-NPs. SiO₂-NPs (100 µg/ml; ~10 nM) were incubated for 15 minutes at 37°C with increasing amounts of the indicated proteins in RPMI 1640. After separation of NPs by ultracentrifugation, the concentration of free proteins left in the supernatants was measured by Bradford assay and plotted against SiO₂-NPs bound proteins, deduced by subtracting free protein from total protein (measured by running mock samples in which the proteins were incubated without NPs and centrifuged in parallel). Data were subjected to non-linear fitting (N=3 for each protein). Dissociation constant (K_d) and the maximal binding capacity (B_{max}, number of protein molecules per NPs), calculated for each protein using a one-site equilibrium equation (see methods), are summarized in the lower table.

Moreover, the found K_d values for Fibr and HSA association to our SiO₂-NPs (28 and > 1000 nM, respectively) also fit with those obtained by Pelaz et al.³⁷ (30 and 1000-4100 nM, respectively) with negatively charged FePt particles variously coated with PMA and PEG, in spite of the different chemical nature of the NPs there used.

Effect of plasma proteins and of their selective lack on SiO₂-NPs dispersion.

Additional interesting information on the specific contribution of the investigated proteins properties to the HP-hard corona on SiO₂-NPs was obtained by measuring their ability to induce nanoparticle aggregation via Dynamic Light Scattering analysis. The presence of a large excess of proteins with size comparable to, or larger than, our NPs prevents the possibility to detect the corona coated nanoparticles and to measure their Z-potential by DLS in the conditions used. Nevertheless, the formation of large protein-nanoparticle aggregates can be detected. When the nanoparticles were incubated at 20 µg/mL with 10% FCS, MP, HP, and the *corona mix*, a mixture made of the main HP corona proteins (see *infra*), they did not produce any observable particle aggregation (Figure 6). Also the selective lack of each of the single protein, included HRG, from the *corona mix* did not induce NPs aggregation (Figure

S7A). On the other hand, when the concentration of the nanoparticles was increased above 100 µg/mL, the formation

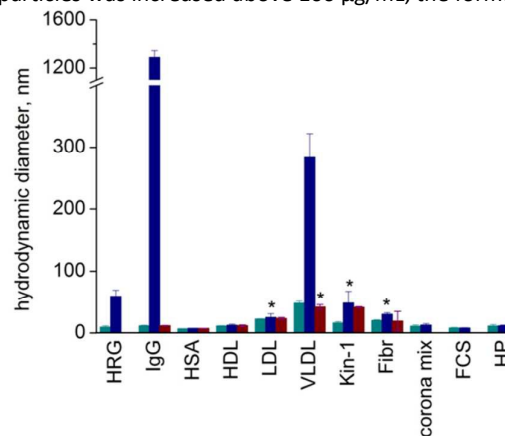


Figure 6. Effect of plasma proteins on SiO₂-NPs aggregation. DLS analysis (PBS buffer pH 7.4, 37°C) of the single purified plasma proteins indicated at the concentration found in 10% HP, the total protein mixture of them (*corona mix*), 10% FCS and 10% HP alone (green bars) or after incubation (10 minutes) with 20 µg/ml SiO₂-NPs in the absence (blue bars) or in the presence (brown bars) of purified HRG (15 µg/ml). Protein concentrations: HRG (15 µg/ml), Kin-1 (8 µg/ml), HDL (150 µg/ml), LDL (78 µg/ml), VLDL (12 µg/ml), HSA (5 mg/ml), IgG (700 µg/ml) and Fibr (300 µg/ml). Secondary populations of NPs/protein aggregates (always below 5%) are indicated, when present, by an asterisk. Data are means ± SE (N=3). Note that for high protein concentrations, corona coated silica nanoparticles cannot be detected due to prevalent scattering by excess free proteins (see experimental part).

of aggregates having an hydrodynamic radius of about 100 nm was observed (Figure S7B) in FCS, HP, *corona mix* but not in MP.

When the single proteins were analysed, we found that incubation of HRG (having an hydrodynamic diameter around 10 nm in DLS analysis) with nanoparticles induces the formation of objects with a mean diameter around 50 nm and a Z-potential of -9.5 mV. Such figures are compatible with the formation of a negatively charged corona of HRG molecules (the isoelectric point of HRG is 5.9-6.2) assembled around monodispersed NPs. Similar results were obtained for Kin-1. IgG and VLDL induced extensive nanoparticle aggregates having an apparent diameter above 1 µm and between 250-350 nm respectively. Fibr and LDL determined only a small subpopulation of aggregated NPs. HSA and HDL did not induce NPs aggregation.

Consistent with its high affinity interaction with the NPs, addition of HRG prevented the aggregation of SiO₂-NPs induced by IgG, VLDL, Fibr and LDL and, as expected, did not modify the already absent aggregation of NPs incubated with HSA, Kin-1 and HDL. These data suggest that, in the absence of HRG, other proteins can prevent particles agglomeration but also further support that HRG can compete with more abundant plasma proteins, as IgG and VLDL, for the NPs surface, inhibiting in this case their aggregating attitude.

From this point of view it may be interesting to note that when SiO₂-NPs are incubated with mouse plasma well above the concentration of 100 µg/ml no protein aggregates are induced (Figure S7B). This finding is in perfect agreement with the

observation that in this medium HRG remains the major corona component even at high NPs doses, differently with

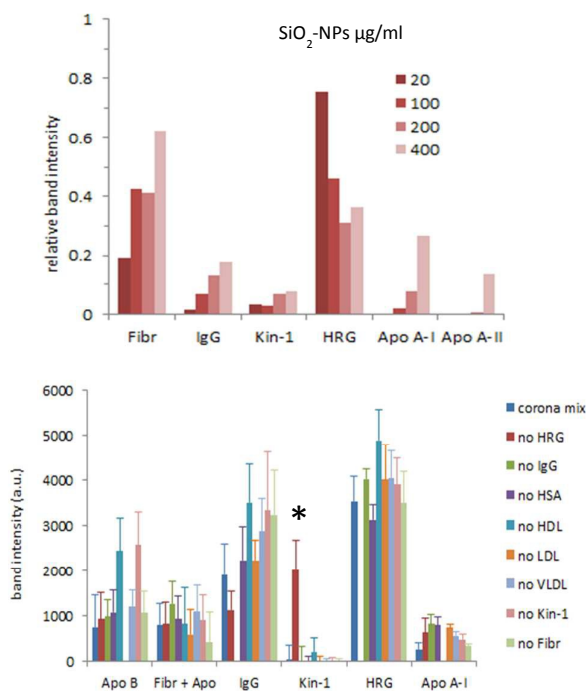


Figure 7. Analysis of the protein hard-corona composition of SiO₂-NPs in the presence of different combinations of purified plasma proteins. A) Composition of the corona formed around SiO₂-NPs incubated at the indicated concentrations in a RPMI 1640 medium characterized by the contemporaneous presence of HRG (15 µg/ml), Kin-1 (8 µg/ml), HDL (150 µg/ml), LDL (78 µg/ml), VLDL (12 µg/ml), HSA (5 mg/ml), IgG (700 µg/ml) and Fibr (300 µg/ml) at concentrations fairly mimicking those found in 10% HP (corona mix). Histograms show the semi-quantitative estimation of the amount of the indicated proteins associated to NPs obtained by densitometry of the corresponding SDS-PAGE bands after silver staining following normalization over the sum of the intensities of all the band of the corresponding run (see Fig. S8A). B) Composition of the coronas formed after incubation of SiO₂-NPs (20 µg/ml) in the presence of the complete corona mix as above or in the presence of the corona mix lacking a single protein of the mixture as indicated. Histograms are the means \pm SE of four different experiments. Representative gels out of eight, are shown in Fig. S8A and B. * significance $p < 0.05$ with respect to corona mix samples.

what found in human plasma (Figure S5D). Taken together, these data support the idea that HRG form a stable and quite homogenous corona and suggest that it may be more concentrated in the mouse blood (similarly to rabbits) than in human ones, and that, for this reason, its protective effect against aggregation is exerted at higher nanoparticles concentrations.

Different intrinsic efficacies of the main plasma proteins found in the HP hard corona of SiO₂-NPs to modulate nanoparticle cell binding.

The main information provided by all the above experiments is that, apparently, a relatively small group of proteins accounts for the major features of the HP-derived protein hard-corona of SiO₂-NPs. However, we can also notice that many among the corona polypeptides identified are apolipoproteins.³⁸⁻⁴⁰ Apo B-100 is found as major component in the proteome of VLDL

(Very Low Density Lipoprotein) and LDL (Low Density Lipoprotein), but is also found as minor component of the HDL

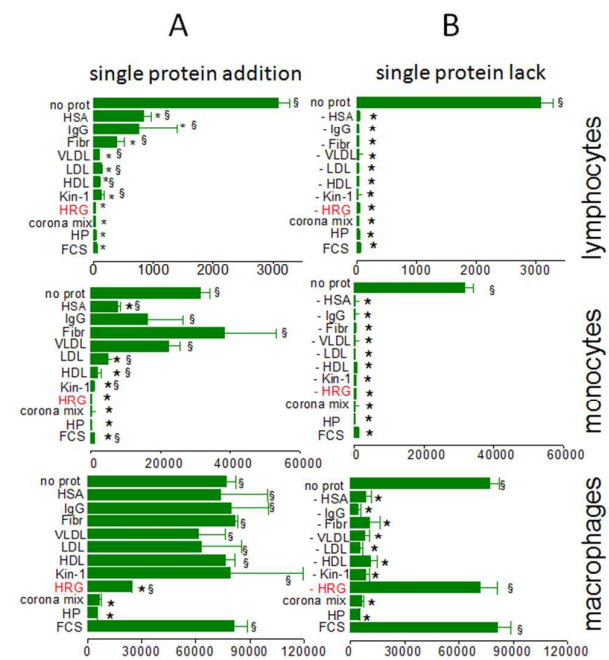


Figure 8. Effect of the main HP-derived corona proteins on SiO₂-NPs capture by lymphocytes, monocytes and macrophages. A) Cells were incubated at 37°C with 20 µg/ml SiO₂-NPs in RPMI 1640 without protein (no prot), plus 10% HP (HP), 10% FCS (FCS) or the indicated purified human plasma proteins alone or all together (corona mix) at concentrations found in 10% HP as already specified in the legend of Figure 6 and 7. After 3 h, cells were analysed by flow-cytofluorimetry to quantify NPs-cell association (MFI). B) The same analysis was performed, in parallel, incubating cells and NPs in the presence of the corona mix with the selective lack of each forming protein, as indicated (- protein). Data are the mean \pm SE of duplicate experiments (N=3). * significance ($p < 0.05$) with respect to no protein; § significance ($p < 0.05$) with respect to HP.

(High Density Lipoprotein) proteome; Apo A-I is the major apolipoprotein of HDL, but can be significantly found in VLDL and in LDL; Apo A-II is the second mostly represented in HDL, but is also detected in VLDL and LDL proteomes; Apo A-IV can be found in HDL, LDL and VLDL proteomes; Apo C-III is present in VLDL as a major protein, while in LDL as minor ones, but is also found in HDL; SAA-4 is similarly found in HDL, LDL and VLDL proteome. In addition, small amounts of Fibrinogen are found in HDL, LDL and VLDL. For this reason, the above indicated markers strongly suggest the involvement, to various extent, of all the three kinds of human plasma lipoprotein classes in the corona of SiO₂-NPs at high nanoparticles doses.

To study in more detail the role of the major human plasma proteins involved in the formation of the corona on SiO₂-NPs, purified human HDL, LDL and VLDL fractions were therefore mixed with purified human plasma IgG fraction (including the four human subclasses of IgG1, IgG2, IgG3, IgG4), HRG, Kin-1, Fibr and HSA at concentrations resembling the mean values present in 10% HP to obtain a simplified protein medium that will be named *corona mix* for the rest of the study.

The analysis of the composition of the corona formed upon incubation of the nanoparticles with the *corona mix* revealed a polypeptide composition very similar to that observed when

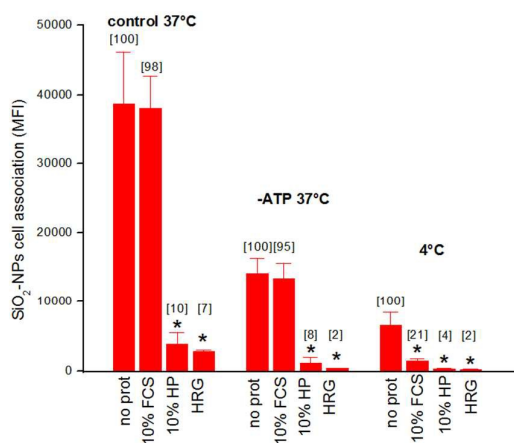


Figure 9. Effect of energy depletion and low temperature on the SiO₂-NPs association to macrophages. Macrophages were pre-treated or not for 30' at 37°C with sodium azide 10mM plus 2-DG 5 mM to deplete ATP (-ATP) in the presence of RPMI 1640 without protein (no prot), with 10% FCS, 10% HP or 15 µg/ml HRG (corresponding to its concentration in 10% HP). Then, SiO₂-NPs 20 µg/ml were added for 2 hours both at 37°C or 4°C. After incubation, cells were washed and analysed by flow-cytometer to quantify NPs-cell association (MFI). Data are the mean ± SE of three experiments run in duplicate. Numbers in brackets and * are % and significance (p<0.05) with respect to no prot samples in each condition.

HP is used (Figure 7A, Figure S8A). Moreover, uptake experiments with macrophages demonstrated that the protective effect of HP, at low nanoparticles concentration, is maintained to a similar extent when the *corona mix* is used as protein source (Figure S8C). Both these results confirm that the proteins selected in the corona mix are the relevant actors at play in the corona formation and in the nanoparticle-macrophages interaction.

In line with the above measured affinities, the selective lack of HRG from the *corona mix*, at 20 µg/ml nanoparticles concentration, resulted into an improved recruitment of the homologous Kin-1 on NPs (Figure 7B, Figure S8B). On the contrary, the lack of all other proteins did not significantly modify the corona composition, which continued to be mostly characterized by a high HRG prevalence.

The ability of the *corona mix* to reproduce the effect of HP on the nanoparticles behaviour, allowed the systematic analysis the intrinsic ability of each protein to modulate the association of SiO₂-NPs to lymphocytes, monocytes and macrophages. When each protein was tested separately, distinctive differences were found in the three cell types (Figure 8A). In the case of lymphocytes, any protein decreased SiO₂-NPs cell-association. In detail, HSA, IgG and Fibr strongly diminished NPs binding (75-80% inhibition) while lipoproteins (HDL, LDL, VLDL), HRG and Kin-1 determined an almost complete block of NPs binding. In monocytes, Fibr slightly stimulated NPs cell binding, IgG and VLDL had no significant effect and HSA and LDL were partially inhibitory (80-90% inhibition). On the other hand, HDL, HRG and Kin-1 decreased the binding of NPs to

monocytes to values smaller than that induced by FCS and similar to HP. Finally, the most peculiar situation was observed in macrophages, where only HRG could inhibit NPs cell association (80% inhibition) and none of the other proteins, included the homologous Kin-1, had a significant inhibitory effect. Dose response analysis confirmed that this inhibitory effects are maintained in the 5-40 µg/ml SiO₂-NPs concentration interval (Figure S9).

The above experiments indicate that, while several plasma proteins may potentially inhibit NPs uptake by lymphocytes and monocytes, only HRG seems to account for the observed inhibitory effect of HP on macrophages. To further investigate this hypothesis, we incubated the cells in the presence of the whole *corona mix* and tested the effect determined by the selective omission of a single protein from the mixture (Figure 8B). This experiment measures the real contribution of a given protein in the presence of the other major ones, taking into account all the reciprocal protein-protein competition and interactions that may be crucial to determine the final functional outcome. The results obtained again showed a peculiar distinction of macrophages from the other two cell types and confirm the specific protective effect of HRG. In lymphocytes and monocytes the lack of each single protein never reverted significantly the cell binding inhibition observed in the presence of the corona mix. On the contrary, in macrophages a complete recovery of the NPs cell association was only obtained when HRG was omitted from the corona mix.

To ascertain what step of cell association is inhibited by HRG, *i.e.* the surface binding or the subsequent cellular endocytosis, we performed experiments in which macrophages were incubated with SiO₂-NPs in no protein, FCS, HP and purified HRG after energy depletion or at 4°C, two conditions that allow plasma membrane binding but block endocytosis. FACS analysis showed that both HP and HRG inhibited cell association when internalization was blocked, while FCS was not or less inhibitory in the same conditions (Figure 9). This result proves that the diminished macrophage accumulation of NPs in the presence of HP and HRG is due to the hampering of cell surface binding, which in turn affects the following active endocytosis of the particles.

SiO₂-NPs are well known to induce cytotoxicity and cytokines release.^{23, 24} No cell death and production of IL-1β was observed in parallel experiments in which cells were treated with SiO₂-NP₅ for 3 hours in the presence of different protein mixtures as above. However, after a prolonged incubation (24 h), we could evaluate the modulatory effect of the various plasma proteins involved in the formation of the HP corona on the intrinsic efficacy of bare NPs to kill cells and to induce IL-1β. The different proteins of the *corona mix* protected cells with different efficacy and selectivity, when used as single agonists: VLDL, LDL, HDL, Kin-1 and HRG are strongly protective in both monocytes and macrophages while HSA, IgG and Fibr are poorly protective in monocytes and protective in macrophages. Consequently, FCS, HP and the *corona mix* all completely inhibited the cytotoxic and pro-inflammatory effects of SiO₂-NPs, and in no case the selective deprivation of

single proteins from the corona mix resulted in the recovery of cytokine production and cell toxicity (Figure S10). This data

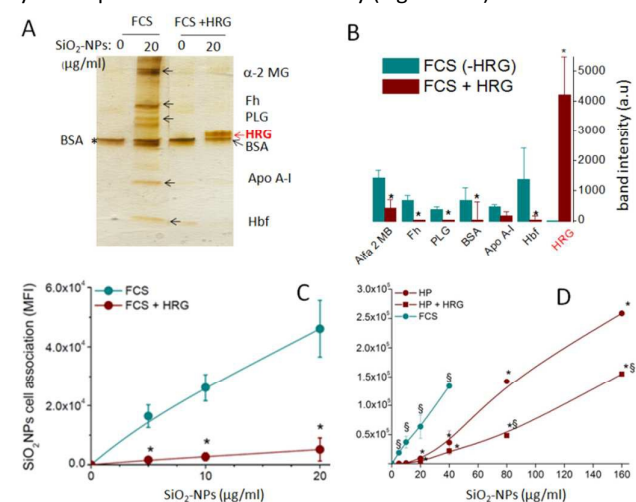


Figure 10. Effect of HRG on the capture of SiO₂-NPs by macrophages in FCS and HP. A) SiO₂-NPs (20 µg/ml) were incubated with 10% FCS or with 10% FCS plus purified human HRG (15 µg/ml) for 15 minutes at 37°C, and the hard-corona was analysed by SDS-PAGE after particles recovery and washing by ultracentrifugation (a representative gel out of three is shown). The single bands corresponding to the indicated major proteins, validated by MS, were quantified by densitometry after silver staining, as reported in panel B. BSA non-specific signal, marked in mock (no NPs) SDS-PAGE samples is indicated by an asterisk in the gel. Data are means ± SE (N=3). * significance (p<0.05) compared to HRG lacking conditions. C, D) Macrophages were incubated with SiO₂-NPs at the indicated doses in RPMI with 10% FCS and 10% FCS + 15 µg/ml HRG (C) or in 10% FCS, 10% HP and 10% HP + 15 µg/ml HRG (D) for 3h at 37°C. NPs association to cells was determined after washing by flow-cytofluorimetry. Data are the mean ±SE of three experiments run in duplicate. * significance (p<0.05) compared to FCS; § significance (p<0.05) compared to HP.

suggest that, at least at the relatively low NPs dose used in this study, a specific protein corona composition is not required to block the toxic and proinflammatory effects of SiO₂-NPs and that many different proteins can ensure a non-specific protection of the membrane-active silica surface of NPs.

If HRG is the protein responsible for the protective effect of HP toward macrophage uptake, when it is predominately present in the corona, its absence in FCS may explain the effective capture of SiO₂-NPs by macrophages in this medium. Consequently, we decided to test the effect of the addition of human HRG to FCS at a concentration equivalent to that present in HP. Regarding the corona composition, an almost total displacement of FCS-derived typical proteins (α₂-macroglobulin, Apo A-I, haemoglobin α/β) was observed and HRG became the major protein as in HP (Figure 10A, B). Consistently, a strong reduction of NPs capture by macrophages in FCS implemented with HRG was observed (Figure 10C). Also the addition of purified HRG (+ 30 µg/ml) to HP determined a further improved reduction of SiO₂-NP₃ macrophage capture (Figure 10D). Moreover, HRG indeed completely restored the ability of HRG/Kin-1 depleted HP to inhibit NPs macrophage capture (Figure 11C). Other control experiments in which NPs were incubated with macrophages in the presence of plasma depleted of Fibr, a major protein taking part to the corona after HRG, showed no significant variation of HRG content in the corona and a conserved ability

to inhibit the NPs capture by cells (Figure S11). Another interesting

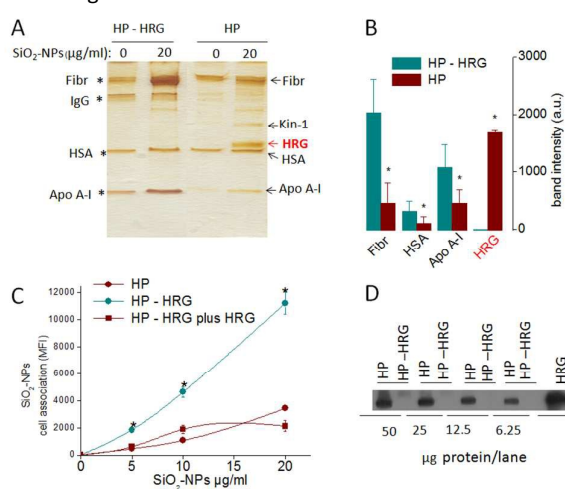


Figure 11. Effect of HRG depletion on the ability of HP to inhibit SiO₂-NPs capture by macrophages. A) SiO₂-NPs (20 µg/ml) were incubated with normal (HP) or HRG-depleted 10% HP (HP-HRG) for 15 min at 37°C. The hard-corona was analysed by SDS-PAGE (representative of three) after particles washing by ultracentrifugation and the main proteins (indicated by arrows and validated by MS) were quantified by densitometry after silver staining. Non-specifically recovered proteins (Fibr, IgG, HSA, Apo A-I) from mock (no NPs) samples run in parallel are marked by asterisks in the gel. B) Histograms represent the band intensity of indicated proteins and are the mean of three experiments ± SE. * significance (p<0.05) compared to HRG lacking conditions. C) Macrophages were incubated at 37°C for 3h with SiO₂-NPs at the indicated doses in the presence of RPMI 1640 medium plus 10% HP, 10% HRG-depleted HP or 10% HRG-depleted HP re-integrated with HRG 15 µg/ml, and NPs association to cells was determined after washing by flow-cytofluorimetry. Data are the mean ±SE of three experiments run in duplicate. * significance (p<0.05) compared to a medium containing HRG. D) The removal of HRG from HP was validated by Western Blot by loading on a 12% non-reducing SDS page 50, 25, 12.5 or 6.25 µg of HP and HP - HRG (previously analysed for total proteins concentration by Bradford assay) and 0.675 µg of purified HRG as positive control. The blot was developed using ECL system for 10 seconds.

aspect of this control is the lack of Kin-1 in the corona, likely due to its involvement in the coagulation process and possibly loss in fibrin clots. This observation further confirms the irrelevant contribution of Kin-1 to the ability of plasma to inhibit SiO₂-NPs capture by macrophages.

Discussion

In this study we found further evidence strongly supporting the paradigm that the composition of the *protein corona* is one of the main factors that control the interaction of nanoparticles with cells. We were however interested not only in elucidating the effect of the corona on the nanoparticle biological activity, but also in understanding which are the relevant *in vitro* conditions required to get information predictive of the behaviour of the nanoparticles *in vivo*. The initial idea that prompted this investigation was that the nanoparticles, once injected in the bloodstream, will experience a substantial dilution and will accumulate primarily in the cells deputed to capture foreign entities. Consequently, we pointed our attention on: human plasma, low nanoparticle concentrations and phagocytic cells.

In line with such premises and with previous studies,^{21, 27, 41} we found that the protein hard-corona undergoes dramatic composition changes depending on the protein source selected (FCS or HP). Moreover, we here show that also the nanoparticles concentration is a determinant parameter, as we will discuss in detail later. We identified two groups of 7 and 12 proteins respectively as major constituent of FCS and HP derived coronas. Among them, only Apo A-I, Apo A-II (HDL markers) and albumin (HSA or BSA) are present in both the sets. When the attention is focused only on the most represented proteins, which are α 2-macroglobuline and haemoglobin α/β for FCS and HRG, Kin-1, and Fibr for HP, no overlap is found between the coronas formed in the two media. Strikingly, in FCS, not only Fibr and Kin-1 are not present, due to the involvement of these two proteins in clot formation which is part of the production of such medium, but also HRG is missing. Such absence likely leaves room to other proteins on the NPs whose affinity for silica surface is lower. This is confirmed by the fact that, when HRG is added to FCS, the corona composition changes completely and becomes similar to that formed in HP.

Such a relatively simple composition of the nanoparticle corona may appear in contrast with other reports, where much larger numbers of corona forming polypeptides are identified.^{2, 3, 5, 11-13, 27, 34} However, this disagreement can be in part explained by our choice to focus on abundant corona components, present in stoichiometric ratios, based on the conceivable hypothesis that these are the molecules predominantly influencing the nanoparticles biological behaviour.

Second, in some cases, we aimed at identifying protein families (ig, lipoproteins) using bona fide and well recognized markers, without differentiating all single composing polypeptides or searching for minor proteome components. For example, Apo A-I allowed us to identify the presence of HDL in the corona⁹ in spite of the larger polypeptides set that characterizes these lipoprotein. In facts, the lipoproteins proteoma is formed by at least 40 polypeptides, in part overlapping with the highly heterogeneous coronas recently reported on Au- and SiO₂-NPs.^{5, 11, 12, 38-40} This suggests that the reported complexity of the NPs corona in shotgun experiments, especially for the abundant sub-stoichiometric components, may be due, at least in part, to the contribution of the HDL, LDL and VLDL own proteomes. Another similar case is represented by antibodies: we marked them as IgGs in our study but several polypeptides or virtual polypeptides, generally reported in shotgun proteomics experiments, contribute to the formation of single antibody molecules and to different isotypes (that were indeed identified by us in the corona).

Eventually, special consideration deserves the fact that we performed our experiments at low nanoparticle concentrations: in these highly limiting conditions, only the proteins with the highest affinity for the nanoparticle surface are supposed to effectively bind them, and this is reasonably expected to simplify the corona protein pattern. Indeed, we found that at higher NPs concentrations, both the absolute

number of protein bands in SDS-PAGE analysis and their heterogeneity sensibly increased, in line with other studies.^{2, 11, 13, 42} Such observation is in agreement with our conclusion that the depletion of HRG allows the recruitment of other proteins in the corona. In this respect, it may also be important to note that, at the higher NPs doses, the simple notion of neat hard coronas around individual NPs may be not apt to interpret data. In fact, in line with another study,²⁷ NPs/plasma proteins large aggregates forms above 100 μ g/ml NPs concentrations (Figure S4). This process may lead to non-specific recovery of more plasma components by NPs clusters, either in solution or during the centrifugation step (*entrapment effect*). Moreover, the concept of corona in this conditions may be not useful, especially when proteins of the same size or bigger than the NPs are found, while a heteroaggregation model may be more appropriate.⁴³

A further element to take in consideration are the results obtained by biochemical titration of the maximal amount of protein units which can associate to NPs. In our study we determined, using purified proteins, that the maximal number of proteins that can accommodate on the surface of our 26 nm diameter SiO₂-NPs is about 30 for HRG, 47 for Kin-1 and 27 for Fibr. These data are in line with the quantification of the same proteins in the corona when particles are incubated with HP at low NPs doses (20 HRG plus 7 Kin-1 and 2-3 Fibr, corresponding to 30 total protein molecules). Not only such experimental figures are in agreement with geometric considerations, providing acceptable protein footprint, but they are also in line with previous literature reports. Dell'Orco *et al.*,⁴⁴ based on geometric simulations, estimated the maximal number of HSA (8 nm diameter), HDL (10 nm diameter) and Fibr (16 nm diameter) molecules that can form a corona monolayer around 70 nm diameter co-polymer NPs. Normalizing their estimate for the difference in surface (\sim 7 times larger compared with our 26 nm diameter SiO₂-NPs) a maximal number of 54 HSA, or 37 HDL, or 16 Fibr molecules per particle can be calculated, not far from our estimations. At the end, it becomes quite evident, both on basis of geometry and of the above discussed results, that tens of protein units per particle, and not hundreds, form a corona monolayer around \sim 26 nm diameter NPs.

This specified, we must stress that although other proteins co-migrating with the major protein bands identified were indeed detected by MS (see Table S2) their scores and semi-quantitative label-free estimation (emPAI parameter)³² indicated that they are minor components with respect to the major ones, especially at low NPs concentrations. This tendency was indeed confirmed in various temperature conditions (37 °C vs 4°C), HP percentage (10% vs 100%) and centrifugation protocols used to isolate NPs-corona complexes.

Taking into account all above considerations and evidence, we conclude that the most peculiar distinctive feature of the HP corona (and also of the MP corona) of silica nanoparticles is the prevalent presence of Histidine-Rich Glycoprotein (HRG) at the low nanoparticle concentration conditions (that are likely more representative of *in vivo* situation). With some

differences, possibly due to the use of higher nanoparticles doses and different conditions, this observation is in agreement with those obtained by Monopoli *et al.* studying silica nanoparticles.⁴⁵ Indeed, in experiments in which much larger SiO₂-NPs concentrations were tested (mg/ml range), these authors found that the HP-derived corona is composed by several proteins including Fibr as the major protein but also HRG, Kin-1, IgGs, HSA, PLG and several HDL and LDL markers. Moreover, increasing plasma concentration from 10% to > 55% changed this pattern in such a way that HRG became the major corona protein, followed by Fibr and HSA, a result compatible with our data. It is also to be noted that HRG and Kin-1 were found as major corona components also in the HP corona of negatively charged NPs made of PLGA⁴⁶ and dextran-Iron Oxide.⁴⁷ Such observations suggest that HRG and Kin-1 may have a high affinity for negatively charged surfaces. In the case of our silica nanoparticles, this hypothesis is supported by the nanomolar dissociation constants we measured.

It is also worthy to stress that we always consistently observed a relative poor abundance of serum albumin in any condition tested (HP at both 10 and 100% concentration, HS, FCS and MP), often accounted just by the background residue, in spite of the fact that this protein is the most abundant in plasma/serum and has been reported as major component of the hard corona in SiO₂-NPs and other NPs. The low affinity of HSA for amorphous silica (> 1 μM), similarly seen in other negatively charged nanoparticles^{36,37} is consistent with this finding and somehow questions the inclusion of albumin in the category of hard-corona proteins for SiO₂-NPs, and possibly other negative NPs, where its presence may be due to incomplete washing of the abundant free protein.

The above discussed biochemical abundance of HRG in the SiO₂-NPs corona is sound also because it is consistent with the main functional observation made in this study, namely that HRG was proven to have an intrinsic ability to inhibit the capture of these NPs by macrophages, while several other plasma proteins variously found in the corona have not. HRG abundance simply explains the here shown ability of human plasma to decrease the macrophage capture of these NPs compared to the bare ones. Indeed, the strong inhibitory action of HP corona on the ability of macrophages to capture NPs implies that the protein(s) mediating such effect must be present in large amount in all nanoparticles in solutions. This suggests that, even if minor components may be present in small proportions, or in strong substoichiometric ratios as indicated by other studies,^{5, 12, 34} they are not able to counterbalance the inhibitory effect of HRG. Our data do not exclude that other minor corona components may contribute to the cell interaction of SiO₂-NPs with macrophages, or other cell types, for example favouring, in a positive way, the insurgence of new properties, but point to HRG as a major functional player able to obstacle the interaction of these NPs with macrophages.

Available information on HRG further supports our structural and functional conclusion. In fact HRG, belonging to the type 3 cystatin family,⁴⁸ found in many vertebrates and invertebrates^{49, 50} is formed by two N-terminal cystatin-like domains, a

central histidine-rich region (HRR), containing multiple GHPH tandem repeats flanked by proline-rich regions, and a C-terminal region.⁵⁰⁻⁵² It is crucial to note, from our perspective, that the HRR is responsible for the binding of HRG to negatively charged matrixes like phospho-cellulose, heparin and heparan sulphate and for its antibacterial/antifungal activity.⁵³⁻⁵⁵ Consequently, HRR could be also responsible for the here observed high affinity of HRG for the negatively charged surface of SiO₂-NPs. This hypothesis is supported by the fact that Kin-1, which is the only other type 3 cystatin that contains a HRR, has a similar high affinity for the nanoparticles, and, consequently, not only is present in significant amount on the SiO₂-NPs surface (together with HRG) but also replaces HRG when this is removed from the corona. The other type 3 cystatins present in serum, like Kininogen 2 and fetuins, which do not contain HRR, were not found associated to SiO₂-NPs in the conditions used, strongly suggesting that it is the HRR domain and not the cystatin one that mediates HRG and Kin-1 binding to SiO₂-NPs. Time course experiments show that HRG, and Kin-1, are not displaced from the corona after a prolonged incubation by other plasma proteins and that these proteins remain the major corona components at low NPs doses.

It can also be noted that also the presence of Kin-1 fits with other known properties of SiO₂-NPs. In fact, at high NPs doses, in addition to Kin-1, partially processed as testified by its anomalous electrophoretic migration, Kallikrein and coagulation factor XII (F-XII or Hageman factor) are also present among other minor corona components. These three proteins indeed form a complex called the *contact system* on negatively charged surfaces and trigger the coagulation process.⁵⁶ SERPING1, a negative regulator of F-XII, is also present in the corona as minor constituent. These data are in agreement with functional data showing that amorphous silica can accelerate the coagulation cascade via the contact system.⁵⁷ Our experiments with coagulated plasma, in which not only fibrinogen but also the contact system (Kin-1, Kallikrein and F-XII) is depleted, confirm that these other minor corona components are not involved in inhibiting SiO₂-NPs macrophage capture.

The variation of the SiO₂-NPs corona composition upon dose increase, which undergoes a decrease of HRG and an increase of the other plasma proteins with lower affinities for silica surface, is consistent with the HRG plasma concentration, with its measured affinity and maximal binding capacity for SiO₂-NPs, and with the rough geometric features of nanoparticles and proteins engaged in this interaction. Density of silica nanoparticles prepared with the Stöber method is 2.0 g/ml.³¹ From this value, it is possible to estimate a surface area of 115 m²/g for nanoparticles with a diameter of 26 nm. Using the footprint value of 60 nm² estimated above for one HRG or Kin-1 molecule, it is possible to calculate that 10% HP contains enough HRG or Kin-1 to coat ~ 100 μg/ml of SiO₂-NPs, while HRG alone can coat a surface area corresponding to about 74 μg/ml nanoparticles. Such figures are in agreement with calculations based on experimentally determined maximal binding capacity and affinity of our NPs for HRG (~ 30 molecules of HRG per particle; K_d = 2.4 nM) that predict a

~90% depletion of soluble HRG in 10% HP by 80 $\mu\text{g}/\text{ml}$ NPs (see paragraph 10 of the SI for more details). However, in the complex mixture of HP, other proteins with lower affinity but higher concentration can compete for nanoparticle surface adsorption also before such threshold is reached. Indeed, we found some Fibr molecule in the HP corona also at the lowest NP concentration explored (20 $\mu\text{g}/\text{ml}$). Fibr affinity for the silica nanoparticle is about 10-fold lower than that of HRG and Kin-1, but its concentration is 3-4 folds larger in molar terms. Hence, as long as the nanoparticles concentration increases it can easily adsorb to the fraction of nanoparticle surface no more protected by HRG and Kin-1, progressively diluting these two proteins in the corona. Eventually, at 160 $\mu\text{g}/\text{mL}$ NPs

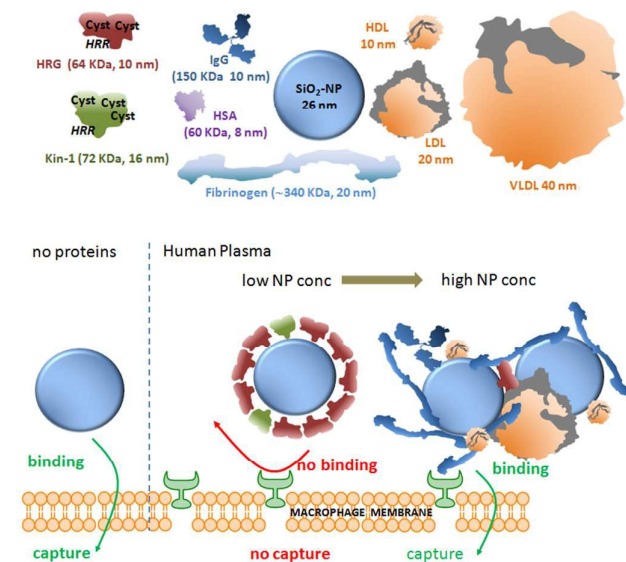


Chart 1. Upper: pictograms of the main proteins engaged in the formation of the concentration-dependent corona of silica nanoparticles in HP. The size and shape of the different proteins were roughly represented in scale to appreciate their dimension with respect to 26 nm diameter SiO_2 -NPs used in this study, also shown. Note that the indicated protein diameters are deduced by DLS measurement done in this study and that especially in the case of Fibrinogen, a fibrillary protein with a length around 40 nm, the value is apparent. The shape of HRG and Kin-1 is an artistic guess based on their secondary structure, in the absence of more detailed information, where Cyst indicates cystatin domains present at the N terminus, while HRR is the cationic Histidine Riche Region likely responsible for the interaction with the negatively charged, silanols containing, surface of SiO_2 -NPs. Lower: uptake of SiO_2 -NPs in the absence of a protein corona (left) or (right) in the presence of a heterogeneous corona (Fibr, HDL, LDL and IgG major proteins here represented-note that HSA is omitted since present in very few amount) formed at high NPs concentrations (here, some degree of particle aggregation is depicted to account for DLS data). Binding and endocytosis inhibition of monodispersed NPs having a uniform HRG-rich corona formed at low NPs concentrations, with a minor contribution of Kin-1 (middle). Note that the corona effects are exerted at the level of plasma membrane binding, non-specific for naked NPs or mediated by macrophagic scavenger receptors for HP coronas at high NPs concentrations, which allows the subsequent energy-dependent capture of the NP (see text for thorough discussion).

concentration, the corona is formed by other proteins and, if we consider the protein mass, almost exclusively by large Fibr molecules. Our data predict that other proteins will likely adsorb in sensible amount at larger NP concentrations, when

also Fibr will be depleted from the solution. Such a strong dependence of the corona composition on the nanoparticles concentration is particularly relevant because, over all the proteins tested, HRG is the only one strictly necessary to inhibit the SiO_2 -NPs capture by human macrophages. No other protein, included the structurally related Kin-1, is able to reduce macrophages capture of NPs. The absence of HRG in FCS explains the different uptake behaviour observed in the two media. Remarkably, these results

also show that different compositions of the corona may determine or not different interacting properties of the particles depending on the cell type. Indeed, while the nanoparticle uptake efficacies displayed by monocytes and lymphocytes are very similar in FCS and HP, only using macrophages we could detect a sensibly different uptake which correlates with the different origin of the corona. The choice of the cellular model used for determining the biological behaviour of nanoparticles is hence very important. Macrophages are the main responsible for particulate blood clearance. This selective “stealth effect” of HRG with respect to the nanoparticles capturing ability of primary human macrophages may have important consequences in the bioavailability of SiO_2 -NPs, and, possibly, other negative NPs *in vivo*.

Although the mechanistic explanation of HRG effect will require further investigations, we can already formulate reasonable hypothesis, based on available evidence. Experiments performed at low temperature and upon inhibition of energy dependent processes indicate that HRG prevents the binding of the nanoparticles to the cell plasma membrane, which is the first step of internalization. We’ve already reported that in protein free media the silica nanoparticle bind to cell membranes displaying a relevant membrane disruption activity.^{23, 24} Such non-specific interaction could be considered responsible for the strong capture of the “naked” nanoparticles in all the cell considered. Apparently, the formation of the corona in the absence of HRG is able to prevent nanoparticles association to other cell types with the very exception of macrophages. In this last case, nanoparticles internalization could arise from the presence of specific receptors, as HSA, fibrinogen (MAC-1), HDL scavengers receptors, and Fc receptor capable to recognize the nanoparticle adsorbed proteins (see scheme in Chart 1). This hypothesis may explain why Kin-1 is not able to prevent macrophage capture like its homologous protein HRG. In fact Kin-1 also binds to MAC-1 scavenger receptor present on these cells. Indeed, Mac-1, an integrin heterodimeric receptor expressed in macrophage, known to bind to iC3b-coated target cells, is a multifunctional receptor able to bind also fibrinogen and the Kallikrein cleaved Kin-1 or HKa.⁵⁸

In the case of FCS, it may be useful to note that the most abundant corona protein in this medium, haemoglobin, may bind to scavenger receptor class B type 1 (SR-B1), and CD163 expressed on macrophages.⁵⁹

The fact that SiO_2 -NPs macrophages binding and the following uptake does not occur effectively when the corona is mostly composed by HRG may indicate that these cells do not have

receptors for HRG or, alternatively, that the nanoparticle adsorption may prevent the recognition of HRG, due to unfavourable orientation. Indeed, HRG was reported to mediate the capture of HRG-opsionized dead cells by monocytes, via the link formed by IgG₂,⁶⁰ although other evidence did not support this possibility.⁶¹ We here observed an opposite, anti-opsionic effect of HRG on SiO₂-NPs, not modulated by the presence or the absence of IgG. It is therefore possible that the interaction of HRG with the silica surface is different from that with dead cell surface, so that further binding of IgG₂ is impossible. Other studies showed that HRG also binds fibrinogen.⁶² However, we did not find a positive correlation between HRG and Fibr recruitment in the HP corona, while, on the contrary, fibrinogen binding occurred after the consumption of free HRG at higher NPs doses. Once again, it may be that the ability of HRG to bind Fibr, is compromised in silica-adsorbed HRG. A role in the ability of HRG to inhibit the binding to macrophages may also be played by its glycosylation. In fact, recent observations indicate that glycosylation of the corona associated glycoproteins, among which HRG was indeed also identified as a major constituent, not only stabilizes SiO₂-NPs in solution but also reduces the binding to macrophages,⁴⁰ in good agreement with our data, showing the high prevalence of highly glycosylated HRG in plasma excess and the parallel prevention, in these conditions, of NPs aggregation and macrophage capture by this protein. However, since we have shown that the homologous and as well glycosylated Kin-1, although able to bind effectively to SiO₂-NPs cannot prevent macrophage binding, it seems clear that subtler biochemical, HRG-specific, mechanisms must play a role, as discussed above.

Conclusions

In summary, we here report that a single protein, namely HRG, present in human (and mouse) plasma but not in FCS, is potentially capable to completely change the biological fate of silica nanoparticles by strongly reducing their capture by macrophages. HRG appears to have a high affinity for silica surface, likely arising from its histidine-rich motives, and is able to compete for nanoparticles binding with proteins present in plasma at much higher concentrations. However, the limited plasma concentration of HRG allows for the formation of a homogeneous and stable corona only below a relatively small nanoparticles concentrations. Indeed, a strong assumption of our study is that final low particle concentrations better simulate the *in vivo* situation. Low particle/high protein situations are more plausible in many cases, such as rapid injection in the bloodstream. However, it is also possible that in some circumstances, for example subcutaneous injection, or depending on the NPs system nature, the initial *bolus* of NPs provide enough particles for aggregation to occur before dispersion. So, high NPs dilutions and the corona formed in this case should not be taken as an *a priori* absolute requirement to predict the behaviour of NPs *in vivo*. In other cases, at least in the initial phase, low dilutions may better

represent the situation *in vivo*. In this light, further experiments should be focused on the kinetics of reversion or time evolution of protein-NPs complexes and aggregates initially formed at relatively high NPs concentrations in a given host fluid upon subsequent dilution in the same, or others, physiological solutions. Nevertheless, our data, pointing to the phenomena linked to NPs concentration relative to protein availability, still highlight how only a careful choice of the experimental conditions may allow obtaining *in vitro* results predictive of the general nanoparticle biological behaviour.

In summary, three variables are essential for useful corona functional analysis: 1) the use of an appropriate physiological medium (plasma proteins for NPs envisaged for blood injection), 2) the careful selection of nanoparticles concentration and 3) the use of appropriate cell models. Interspecific differences in HRG plasma concentrations must be also taken into account, as our data obtained in mouse plasma indicate, since this might modify the pharmacokinetics of negatively charged NPs.

Eventually, the results here discussed may also disclose intriguing applications. First, HRG has been shown to regulate haemostasis and to antagonize cancer progression.^{63, 64} Further studies will be required to assess if such effects are retained in the NPs-adsorbed HRG, and can be possibly exploited for medical purposes. Second, our data also suggest the possibility that the stable recruitment of HRG and its further stabilization on the surface of nanosystems could be used as an alternative strategy to obtain a biomimetic and biocompatible "stealth" layer on nanotheranostics.

Experimental Section

Synthesis of fluorescein-apters (FITC-APTES)

Fluorescein isothiocyanate (0.031 mmol) was dissolved in 10 mL of 11 dry tetrahydrofuran (THF) in a flame-dried flask. Then 7.2 μ L of (3-aminopropyl)triethoxysilane (APTES, 0.031 mmol) and 4.3 μ L of triethylamine (0.031 mmol) were added. The mixture was stirred for 16 h at room temperature in N₂ atmosphere (TLC, silica plate, ethyl acetate, R_f = 0.5). The solvent was evaporated and the residue was dissolved in 3 mL of THF. This solution was added dropwise to 20 mL of n-hexane and the precipitated product was recovered by centrifugation (4000 g for 5 minutes). This purification procedure was repeated two times. The product (12 mg) was obtained as of yellow powder (64% yield). ESI-MS *m/z*: [M+H]⁺ calcd for C₃₀H₃₅N₂O₈SSi, 611.2; found, 611.6 (100 %).

Nanoparticles synthesis, characterization and stability

Stöber nanoparticles were prepared as follows: to a thermostated vessel charged with ethanol (20 mL), 500 μ L (2.45 μ mol) of 4.9 mM solution of FITC-APTES in DMSO and 100 μ L (0.45 mmol) of TEOS were added under stirring at 25 °C. In order to initiate the polymerization, 1.2 mL of 7.4 M aqueous solution of ammonia were then added. After 16 hours, the solution was diluted to 80 mL with ethanol and concentrated to the original volume by ultrafiltration through

a regenerated cellulose membrane (cut-off 10 kDa) under nitrogen pressure (4 bar). The procedure was repeated six times. The solution was filtered through a 0.45 μm regenerated cellulose filter to remove the precipitate. The dilution-concentration procedure was then repeated five more times with milliQ water. The resulting solution was filtered through a 0.22 μm regenerated cellulose filter. Fluorescein concentration is determined by its absorbance at 490 nm ($\epsilon=77000$, pH 9.0). Nanoparticles weight concentration is determined by weighting a dried aliquot of the product. The loading of the FITC-APTES-Si in the nanoparticles was $\sim 0.56\%$ (w/w). Residual free FITC in the preparations were always $< 0.35\%$ ($<0.25\ \mu\text{M}$) compared to the amount of FITC coupled to the NPs matrix (76-99 μM), and were not found to significantly contribute to cell fluorescence in FACS experiments (see below). DLS measurements provide an average diameter of $26\pm 3\ \text{nm}$ (number weighted) with a 0.19 PDI (in phosphate-buffered saline [PBS], pH 7.4). The zeta-potential value (same conditions as DLS analysis) is $-18.3\ \text{mV}$. TEM analysis yields a $25\pm 3\ \text{nm}$ diameter in good agreement with the DLS size. NPs batches (2 mg/ml) were stable in milliQ water for at least 2 months.

DLS measurements

Proteins were incubated in PBS (10 mM, pH 7.4) with Stöber nanoparticles (20 $\mu\text{g}/\text{ml}$) at $37^\circ\ \text{C}$ for 10 minutes. Samples were then transferred into a 120 μl quartz cell and submitted to DLS analysis using a Malvern Instruments Zetasizer NanoS apparatus equipped with a 633 nm laser and a Peltier thermostating system. The proteins used were histidine-rich glycoprotein (HRG, 15 $\mu\text{g}/\text{ml}$), immunoglobulins G (IgG, 700 $\mu\text{g}/\text{ml}$), human serum albumin (HSA, 5000 $\mu\text{g}/\text{ml}$), high density lipoproteins (HDL, 150 $\mu\text{g}/\text{ml}$), low density lipoproteins (LDL, 78 $\mu\text{g}/\text{ml}$), very low density lipoproteins (VLDL, 12 $\mu\text{g}/\text{ml}$), Kininogen-1 (Kin-1, 8 $\mu\text{g}/\text{ml}$), and fibrinogen (Fibr) (300 $\mu\text{g}/\text{ml}$). Prolonged incubation times did not lead to further size modifications. Volume weighted distribution analyses were used in order to allow more reliable detection of nanoparticles and aggregates in the presence of large amount of serum proteins (in number-weighted distribution analysis scattering contribution from serum is prevailing over nanoparticles one at low nanoparticles concentrations, while in intensity-weighted distribution scattering from larger aggregates present in even very small amounts is predominant). Note that average size provided by volume weighed distributions are somewhat larger than those provided by number weighted distribution as a results of the third-power dependence of volume over radius. However, in those experiments where the protein concentrations was particularly high (HSA, HDL, IgG, HP, FCS and corona mix) or where protein size is comparable or greater than particles size (VLDL, LDL) the corona-coated nanoparticles, but not larger nanoparticles aggregates, resulted to be undetectable also in the volume weighted analyses. In other experiments, Stöber nanoparticles (100-500 $\mu\text{g}/\text{ml}$) were incubated with 10% v/v FCS, 10% v/v HP or 10% v/v MP diluted in PBS pH 7.4, and DLS analysis was performed as above.

Cells

Peripheral human blood cells and plasmas (see below) utilized in this study derived from healthy blood donors, as anonymously provided by the Transfusional Center of the Hospital of Padova, in compliance with the relevant laws and institutional guidelines. Written informed consent for the possible use of these materials for research purposes was obtained from blood donors by the Transfusional Center. Data related to human samples were all analysed anonymously. Human leukocytes and plasma were not obtained consequently to experimentation on human beings but as a consequence of voluntary and informed blood donation for transfusions: no approval of Ethics Committee is needed in such cases in our institution. Monocytes-enriched preparations were isolated from human buffy coats by centrifugation over a Ficoll-Hypaque step gradient and a subsequent Percoll gradient as described in Tavano *et al.*⁶⁵ After 1h adherence to plastic in RPMI 1640 (Gibco, BRL see SI for full composition description) supplemented with 2% (v/v) FCS (Euroclone, endotoxin $< 0.3\ \text{EU}/\text{ml}$) and antibiotics (100 U/ml penicillin and 100 $\mu\text{g}/\text{ml}$ streptomycin) stimuli were added. Human macrophages were derived from monocytes for 7 days with 100 ng/ml macrophages colony-stimulating factor (M-CSF, Peprotech) in RPMI 1640 plus 20% FCS. Macrophages differentiation was checked by morphological inspection and differential expression of CD14 and CD16 as previously described.²³ Human hepatocellular carcinoma HepG2 cells were maintained in RPMI 1640 medium supplemented with 10% FCS + antibiotics and split every 2-3 days. All cells were kept at $37^\circ\ \text{C}$ in a 5% CO_2 humidified atmosphere.

Human plasma, human serum, mouse plasma and proteins

Pooled platelet poor human plasma from healthy donors (HP) supplemented with 22 % v/v of citrate phosphate dextrose adenine solution (CPDA-1) as anticoagulant (composition SI) was kindly provided by Centro Trasfusionale of the Hospital of Padua (ULSS16), frozen in aliquots in liquid nitrogen and stored at $-20^\circ\ \text{C}$. Human serum (used as Fibrinogen depleted plasma) was from TCS Biosciences, frozen in aliquots in liquid nitrogen and stored at $-20^\circ\ \text{C}$. Mouse plasma was obtained from freshly drawn mouse blood (containing 0.38% v/v sodium citrate as anticoagulant) after centrifugation at 1,800 g for 10 minutes without accelerator and brake and subsequent spin at 15,000 g for 2 minutes to remove contaminant cells and debris. After freezing in liquid nitrogen, plasma aliquots were stored at $-20^\circ\ \text{C}$. To minimize the formation of Fibr/Fibronectin rich protein cryoprecipitate from plasmas, which forms when this is thawed at low temperature, frozen HP and MP aliquots were always thawed in water bath at $37^\circ\ \text{C}$ and then brought to desired temperatures, depending on the experiment.⁶⁶ Histidine-rich glycoprotein (HRG) was purified from human plasma (see HRG purification). Human immunoglobulin G pool (IgG) and human albumin (HSA) were purchased by Sigma Aldrich, human high, low and very low density lipoproteins (HDL, LDL, VLDL), human High Molecular Weight Kininogen (HMWK or Kininogen 1) and human fibrinogen (Fibr) were from Calbiochem. In DLS, corona and cellular experiments, all proteins were used at concentrations \sim corresponding to 10%

(v/v) human plasma: HRG 15 $\mu\text{g/ml}$; IgG 700 $\mu\text{g/ml}$; HSA 5 mg/ml; HDL 150 $\mu\text{g/ml}$; LDL 78 $\mu\text{g/ml}$; VLDL 12 $\mu\text{g/ml}$; Kin-1 8 $\mu\text{g/ml}$; Fibr 300 $\mu\text{g/ml}$. HP was depleted of HRG and KIN-1 by passing through a phosphocellulose matrix (see HRG purification) and by collecting the flow-through. After dialysis of 3 ml of plasma against 500 ml PBS at 4°C for 18 h (PBS was changed after 3-4 h), the HRG/Kin-1 depleted plasma was quantitated for protein concentration and its activity was compared with normal HP similarly treated and dialyzed, normalizing for protein concentration differences. Dialyzed normal and HRG/Kin-1 depleted human plasma were supplemented with sodium citrate (0.38% v/v) to avoid coagulation and immediately used for cellular treatment or corona experiments.

FACS analysis

Monocytes and macrophages (2×10^6 cells/well; 1×10^6 cells/cm²) seeded into 24-wells plates (Falcon) were incubated at 37°C for 3, 6 or 24 h with Stöber NPs (range: 0-80 $\mu\text{g/ml}$) in different conditions as indicated in figures. In other experiments, macrophages were pre-treated or not for 30' at 37°C with fresh prepared 10 mM sodium azide (Sigma Aldrich) plus 5 mM 2-deoxyglucose (Sigma Aldrich) in the presence of RPMI, RPMI+10% FCS, RPMI+10% HP or RPMI+15 $\mu\text{g/ml}$ HRG. Then, Stöber NPs (20 $\mu\text{g/ml}$) were added for 2 h at 37°C or 4°C. HepG2 cells (1.5×10^5 cells/well) were seeded into 24-wells plates the day before the experiment, and treated at 37°C with Stöber NPs (0-50 $\mu\text{g/ml}$) for 20 h in RPMI, RPMI+10% FCS, RPMI+10% HP. Cells were collected by plastic scraping (monocytes/macrophages) or trypsinisation (HepG2), washed with PBS, resuspended in cold FACS buffer (PBS, pH 7.4 + 1% FCS) supplemented with NH₄Cl 10 mM to neutralize acidic compartments and obtain the maximal FITC fluorescence, and stained with propidium iodide 15 $\mu\text{g/ml}$ (Sigma Aldrich) to exclude dead cells. Samples were acquired with a BD FACSCanto II using a FACSDiva software (Becton Dickinson) and NPs association to alive cells (10,000 events) was evaluated as mean fluorescence intensities (MFI). The contribution of traces of free FITC in the NPs preparations (<0.35% of particle coupled FITC) was estimated testing cells in the same conditions with equivalent quantities of NPs ultra filtrates and found to account for < 0.005% of the signal obtained using the corresponding FITC-labelled NPs preparations.

SiO₂-NPs protein corona determination

Stöber NPs were incubated under stirring at 37°C or 4°C for 15', 3 h and 6 h in RPMI 1640 supplemented with 10% FCS, 10% or 100% HP or 10% MP (thawed at 37°C and pre-centrifuged at 15,300 g for 10' at 4°C to eliminate any aggregates), or the corona mix complete or depleted of each single protein (volume 1.5 - 2 ml). NPs were subsequently diluted with 9 ml of ice-cold PBS pH 7.4 in polycarbonate tubes (Beckman Coulter, cat number 355603), immediately recovered by ultracentrifugation (45 minutes, 100,000 g at 4°C, XL-70 Ultracentrifuge Beckman, fixed angle 50 Ti rotor), washed twice with 10.5 ml of ice-cold PBS pH 7.4 and

eventually dissolved in 75 μl of non-reducing loading sample buffer (62.5 mM Tris-HCl, pH 6.8, 2% SDS, 25% glycerol, 0.01% bromophenol blue). In separate experiments the NPs yields after washings was estimated by comparing the absorbance of FITC in supernatants and the final pellets and found to be $95.5\% \pm 4$ (mean \pm SE; N=6) of the total particles present before centrifugation. In other experiments, SiO₂-NPs protein corona was determined as described in Tenzer *et al.*¹² Briefly, Stöber NPs 20 $\mu\text{g/ml}$ were incubated for 15' at 37° or 4°C in 10% or 100% pre-centrifuged HP in a volume of 2 ml, stratified onto a sucrose cushion (0.7 M in PBS, 2 ml) and centrifuged for 45' at 100,000 g at 4°C using a swing out SW60 Ti rotor (Beckman Coulter) in 4 ml tubes (Beckman Coulter, cat number 344062). After washing twice with 4 ml PBS and centrifuging as above, NPs pellet was dissolved in loading sample buffer. After heating at 95°C for 5' equal volumes (25 μl) or equal amounts (13.3 μg) of samples were subjected to gradient SDS-PAGE in 4-20% Mini-PROTEAN[®] TGXTM Precast Gel (Biorad). Mock samples were always performed using different protein mixtures or FCS/HP protein in the absence of NPs, to estimate nonspecific protein background. Proteins were stained with silver nitrate or with colloidal Coomassie G-250 in case of mass spectrometry analysis, or transferred on a PVDF membrane for Western Blot (see supplementary methods). Band intensities of NPs associated proteins were estimated using Image J software after subtraction of any background signal (mock samples). Serial dilution of known amounts of purified human plasma proteins were loaded in parallel in the same gel to obtain a calibration curve that allowed us to estimate the nmoles of each single protein associated to given amount of NPs nmoles corrected for the NPs recovery after ultracentrifugation (a molecular weight of $\sim 10^7$ Da was assumed for SiO₂-NP; three Apo A-I polypeptides were assumed to be present in one HDL lipoprotein.). This allowed the quantification, after silver staining and densitometry, of the number of protein molecules per corona units.

In-Gel Digestion, Protein identification and Database Search

Excised from the gel, bands were washed with 50% v/v acetonitrile (ACN) in 0.1 M NH₄HCO₃, and vacuum-dried. For the faintest bands two bands from identical parallel lanes were extracted. The proteins were reduced for 30 min at 56°C with 10 mM DTT in 0.1 M NH₄HCO₃. After cooling, the DTT solution was immediately replaced with 55 mM iodoacetamide in 0.1 M NH₄HCO₃ to alkylate the free SH groups for 20 min at 25°C in the dark. After washing with 50% ACN in 0.1 M NH₄HCO₃, the dried gel pieces were swollen in 15 μl of digestion buffer containing 25 mM NH₄HCO₃ and 12.5 ng/ μl trypsin (Promega, Madison, WI, USA) and incubated overnight at 37°C. Tryptic peptides were extracted according to the protocol described by Kim *et al.*²⁶ Peptide mixtures were then analysed by LC MS/MS on a 6520 Q-TOF mass spectrometer (Agilent Technologies, Santa Clara, CA, USA) coupled to a chip-based chromatographic interface. Column volume loading varied from 1 to 4 microliters depending on the staining intensity of the corresponding treated bands, to ensure comparable

analysis. A Large Capacity Chip (C18, 150 $\mu\text{m} \times 75 \mu\text{m}$) with an enrichment column (C18, 9 mm, 160 nl volume) was used to separate peptides at a flow rate of 0.3 $\mu\text{l}/\text{min}$. Water/formic acid 0.1% and acetonitrile/formic acid 0.1% were used as eluents A and B, respectively. The chromatographic separation was achieved with a gradient of B from 5% to 50% in 20 min. Raw data files were converted into Mascot Generic Format (MGF) with MassHunter Qualitative Analysis Software version B.03.01 (Agilent Technologies) and analysed with Mascot Search Engine version 2.2.4 (Matrix Science). MS/MS spectra were searched against the SwissProt database, with the Mammalia taxonomy filter (June 2014 version, Taxonomy Mammalia, 66370 peptide entries). Enzyme specificity was set to trypsin/P with 2 missed cleavage, using a mass tolerance window of 20 ppm for parent mass and 0.6 Da for fragment ions. Carbamidomethylation of cysteine was set as fixed modification and methionine oxidation as variable modification. Proteins were considered positive hits if at least 2 peptides per protein were identified with high confidence ($p < 0.05$). The Exponentially Modified Protein Abundance Index (emPAI) was considered in order to calculate an approximate, label free, relative quantitation of the proteins.³⁰ The emPAI is calculated automatically by Mascot, $\text{emPAI} = 10^{(\text{N}_{\text{observed}}/\text{N}_{\text{observable}}) - 1}$ where *Nobservable* corresponds to the possible peptides hits generated by a given polypeptide based on *in silico* trypsinisation. Label free emPAI values were used, after correction for sample loading (number of bands, volume loaded for LC MS/MS) to calculate the molar % distribution of the main found proteins within the same SDS-PAGE lanes.

HRG purification

Human HRG was purified from human plasma as previously described^{67, 68} using a Fast Liquid chromatography (FPLC) system (Pharmacia). Briefly, 20 ml of a phosphocellulose resin (P11, Whatman) were equilibrated over night at 4°C with 10 volumes of loading buffer (10 mM sodium phosphate, 0.5 M NaCl, 1 mM EDTA, pH 6.8) supplemented with a protease inhibitors cocktail (Roche, cat. number 11873580001). Human plasma (50 ml) was centrifuged (12,000 rpm 20' 4°C), diluted 1:1 with loading buffer 2X, passed through the equilibrated column, and flow through was collected. After extensive washing (20 volumes) with 10 mM sodium phosphate, 0.8 M NaCl, 1 mM EDTA, pH 6.8, bound HRG was eluted by a progressive saline gradient (from 0.8 M to 2 M NaCl) in the absence of protease inhibitors. HRG positive fractions (detected by silver staining and western blot analysis using anti HRG mouse polyclonal antibody (Abnova, B01P) (see Figure S12) were dialyzed at 4°C for 20 h against 20 volumes of PBS pH 7.4, quantified with Bradford assay⁶⁹ using a Bio-Rad Protein Assay Dye reagent and stored in aliquots at -80°C after freezing in liquid nitrogen. On average, 2.4-4.3 mg of protein were obtained from 50 ml human plasma. Thawed HRG aliquots were never re-frozen and re-used for experiments.

Determination of the Kd of protein-SiO₂-NPs complexes

Increasing concentrations of purified human plasma proteins (HRG MW 64 KDa, Kin-1 MW 72 KDa, Fibr MW 340 KDa and

HSA 60 KDa) were incubated with no particles or with SiO₂-NPs (100 $\mu\text{g}/\text{ml} \sim 10 \text{ nM}$, assuming a nanoparticle MW of $\sim 10^7 \text{ Da}$) in PBS pH 7.4 at 37°C for 15 min. After ultracentrifugation for 60 min at 100,000 g using an Optima Max-E Ultracentrifuge (Beckman), the concentration of free proteins in the supernatants (Pr^{f}) were measured by a Bradford colorimetric protein micro-assay. Kd and maximal binding capacity were obtained by plotting particle bound vs free protein concentration (nM) and best fitting non-linearly the data with the one-site equilibrium equation $\text{Pr}^{\text{b}} = \text{Pr}^{\text{f}} \text{Pr}^{\text{b}}_{\text{max}} / (\text{Pr}^{\text{f}} + \text{Kd})$ (Origin mathematics package), where Pr^{b} is SiO₂-NPs bound protein concentration, $\text{Pr}^{\text{b}}_{\text{max}}$ is the maximal bound protein concentration and Kd is the dissociation constant.

Statistical analysis

Statistical analyses were performed using the Microcal Origin 8 software package. Gaussian distribution of data was checked by Shapiro-Wilk test (0.05 level). Significance of the differences between means (0.05 level) was evaluated by two samples or paired t test, when applicable, by ANOVA analysis.

Acknowledgements

We thank the Centro Trasfusionale of the Hospital of Padua (ULSS 16) for providing buffy coats and human plasma, Dr. Paolo di Muro for HRG purification assistance and dr. Giovanni Miotto (Proteomics Facility of the University of Padua) for technical assistance in mass-spectrometry analyses.

This work was supported by the European Community's Seventh Framework Programme (FP7/2007-2013) under grant agreement no. 201031 NANOPHOTO, by the University of Padova (Ex 60%, 2010-2014, PRAT 2011, Progetto Strategico NAMECA) and by the Italian Ministry of Research (FIRB 2011, RBAP114AMK-RINAME).

Notes and references

- 1 P. Aggarwal, J. B. Hall, C. B. McLeland, M. A. Dobrovolskaia and S. E. McNeil, *Adv. Drug Deliv. Rev.*, 2009, **61**, 428-437.
- 2 M. Lundqvist, J. Stigler, T. Cedervall, T. Berggard, M. B. Flanagan, I. Lynch, G. Elia and K. Dawson, *ACS Nano*, 2011, **5**, 7503-7509.
- 3 M. Lundqvist, J. Stigler, G. Elia, I. Lynch, T. Cedervall and K. A. Dawson, *Proc. Natl. Acad. Sci. U. S. A.*, 2008, **105**, 14265-14270.
- 4 N. P. Mortensen, G. B. Hurst, W. Wang, C. M. Foster, P. D. Nallathamby and S. T. Retterer, *Nanoscale*, 2013, **5**, 6372-6380.
- 5 C. D. Walkey, J. B. Olsen, F. Song, R. Liu, H. Guo, D. W. Olsen, Y. Cohen, A. Emili and W. C. Chan, *ACS Nano*, 2014, **8**, 2439-2455.
- 6 Z. J. Deng, M. Liang, I. Toth, M. Monteiro and R. F. Minchin, *Nanotoxicology*, 2013, **7**, 314-322.
- 7 A. Gessner, A. Lieske, B. R. Paulke and R. H. Muller, *J. Biomed. Mater. Res. A.*, 2003, **65**, 319-326.
- 8 A. Gessner, R. Waicz, A. Lieske, B. Paulke, K. Mader and R. H. Muller, *Int. J. Pharm.*, 2000, **196**, 245-249.

- 9 T. Cedervall, I. Lynch, M. Foy, T. Berggard, S. C. Donnelly, G. Cagney, S. Linse and K. A. Dawson, *Angew. Chem. Int. Ed Engl.*, 2007, **46**, 5754-5756.
- 10 R. R. Arvizo, K. Giri, D. Moyano, O. R. Miranda, B. Madden, D. J. McCormick, R. Bhattacharya, V. M. Rotello, J. P. Kocher and P. Mukherjee, *PLoS One*, 2012, **7**, e33650.
- 11 S. Tenzer, D. Docter, S. Rosfa, A. Wlodarski, J. Kuharev, A. Rekić, S. K. Knauer, C. Bantz, T. Nawroth, C. Bier, J. Sirirattanapan, W. Mann, L. Treuel, R. Zellner, M. Maskos, H. Schild and R. H. Stauber, *ACS Nano*, 2011, **5**, 7155-7167.
- 12 S. Tenzer, D. Docter, J. Kuharev, A. Musyanovych, V. Fetz, R. Hecht, F. Schlenk, D. Fischer, K. Kiouptsi, C. Reinhardt, K. Landfester, H. Schild, M. Maskos, S. K. Knauer and R. H. Stauber, *Nat. Nanotechnol.*, 2013, **8**, 772-781.
- 13 C. D. Walkey, J. B. Olsen, H. Guo, A. Emili and W. C. Chan, *J. Am. Chem. Soc.*, 2012, **134**, 2139-2147.
- 14 D. Walczyk, F. B. Bombelli, M. P. Monopoli, I. Lynch and K. A. Dawson, *J. Am. Chem. Soc.*, 2010, **132**, 5761-5768.
- 15 R. Huang, R. P. Carney, F. Stellacci and B. L. Lau, *Nanoscale*, 2013, **5**, 6928-6935.
- 16 U. Sakulku, L. Maurizi, M. Mahmoudi, M. Motazacker, M. Vries, A. Gramoun, M. G. Ollivier Beuzelin, J. P. Vallee, F. Rezaee and H. Hofmann, *Nanoscale*, 2014, **6**, 11439-11450.
- 17 S. Winzen, S. Schoettler, G. Baier, C. Rosenauer, V. Mailaender, K. Landfester and K. Mohr, *Nanoscale*, 2015, **7**, 2992-3001.
- 18 R. Liu, W. Jiang, C. D. Walkey, W. C. Chan and Y. Cohen, *Nanoscale*, 2015, **7**, 9664-9675.
- 19 M. A. Malvindi, V. Brunetti, G. Vecchio, A. Galeone, R. Cingolani and P. P. Pompa, *Nanoscale*, 2012, **4**, 486-495.
- 20 F. D. Sahneh, C. M. Scoglio, N. A. Monteiro-Riviere and J. E. Riviere, *Nanomedicine (Lond)*, 2014, **9**, 1-9.
- 21 A. Lesniak, F. Fenaroli, M. P. Monopoli, C. Aberg, K. A. Dawson and A. Salvati, *ACS Nano*, 2012, **6**, 5845-5857.
- 22 N. A. Monteiro-Riviere, M. E. Samberg, S. J. Oldenburg and J. E. Riviere, *Toxicol. Lett.*, 2013, **220**, 286-293.
- 23 C. Fedeli, D. Segat, R. Tavano, G. De Franceschi, P. P. de Laureto, E. Lubian, F. Selvestrel, F. Mancin and E. Papini, *Nanomedicine (Lond)*, 2014, **9**, 2481.
- 24 C. Fedeli, F. Selvestrel, R. Tavano, D. Segat, F. Mancin and E. Papini, *Nanomedicine (Lond)*, 2012, **8**, 1101.
- 25 Y. Yan, K. T. Gause, M. M. Kamphuis, C. S. Ang, N. M. O'Brien-Simpson, J. C. Lenzo, E. C. Reynolds, E. C. Nice and F. Caruso, *ACS Nano*, 2013, **7**, 10960-10970.
- 26 J. A. Kim, A. Salvati, C. Aberg and K. A. Dawson, *Nanoscale*, 2014, **6**, 14180-14184.
- 27 E. Izak-Nau, M. Voetz, S. Eiden, A. Duschl and V. F. Puentes, *Part Fibre Toxicol.*, 2013, **10**, 56-8977-10-56.
- 28 T. M. Forte, J. J. Bell-Quint and F. Cheng, *Lipids*, 1981, **16**, 240-245.
- 29 W. Stöber, A. Fink and E. Bohn, *Journal of colloid and interface science*, 1968, **26**, 62-69.
- 30 A. Van Blaaderen and A. Vrij, *Journal of colloid and interface science*, 1993, **156**, 1-18.
- 31 A. Van Blaaderen and A. Vrij, *Langmuir*, 1992, **8**, 2921-2931.
- 32 Y. Ishihama, Y. Oda, T. Tabata, T. Sato, T. Nagasu, J. Rappsilber and M. Mann, *Mol. Cell. Proteomics*, 2005, **4**, 1265-1272.
- 33 A. K. Rai, B. Spolaore, D. A. Harris, F. Dabbeni-Sala and G. Lippe, *J. Bioenerg. Biomembr.*, 2013, **45**, 569-579.
- 34 M. P. Monopoli, D. Walczyk, A. Campbell, G. Elia, I. Lynch, F. B. Bombelli and K. A. Dawson, *J. Am. Chem. Soc.*, 2011, **133**, 2525-2534.
- 35 C. Rocker, M. Potzl, F. Zhang, W. J. Parak and G. U. Nienhaus, *Nat. Nanotechnol.*, 2009, **4**, 577-580.
- 36 P. Maffre, S. Brandholt, K. Nienhaus, L. Shang, W. J. Parak and G. U. Nienhaus, *Beilstein J. Nanotechnol.*, 2014, **5**, 2036-2047 (DOI:10.3762/bjnano.5.212 [doi]).
- 37 B. Pelaz, P. Del Pino, P. Maffre, R. Hartmann, M. Gallego, S. Rivera-Fernandez, J. M. de la Fuente, G. U. Nienhaus and W. J. Parak, *ACS Nano*, 2015, **9**, 6996-7008 (DOI:10.1021/acsnano.5b01326 [doi]).
- 38 A. S. Shah, L. Tan, J. L. Long and W. S. Davidson, *J. Lipid Res.*, 2013, **54**, 2575-2585.
- 39 T. Vaisar, S. Pennathur, P. S. Green, S. A. Gharib, A. N. Hoofnagle, M. C. Cheung, J. Byun, S. Vuletic, S. Kassim, P. Singh, H. Chea, R. H. Knopp, J. Brunzell, R. Geary, A. Chait, X. Q. Zhao, K. Elkon, S. Marcovina, P. Ridker, J. F. Oram and J. W. Heinecke, *J. Clin. Invest.*, 2007, **117**, 746-756.
- 40 M. Dashty, M. M. Motazacker, J. Levels, M. de Vries, M. Mahmoudi, M. P. Peppelenbosch and F. Rezaee, *Thromb. Haemost.*, 2014, **111**, 518-530.
- 41 S. Laurent, C. Burtea, C. Thirifays, F. Rezaee and M. Mahmoudi, *J. Colloid Interface Sci.*, 2013, **392**, 431-445.
- 42 S. Wan, P. M. Kelly, E. Mahon, H. Stockmann, P. M. Rudd, F. Caruso, K. A. Dawson, Y. Yan and M. P. Monopoli, *ACS Nano*, 2015, **9**, 2157-2166.
- 43 W. Liu, J. Rose, S. Plantevin, M. Auffan, J. Y. Bottero and C. Vidaud, *Nanoscale*, 2013, **5**, 1658-1668.
- 44 D. Dell'Orco, M. Lundqvist, C. Oslakovic, T. Cedervall and S. Linse, *PLoS One*, 2010, **5**, e10949.
- 45 M. P. Monopoli, D. Walczyk, A. Campbell, G. Elia, I. Lynch, F. B. Bombelli and K. A. Dawson, *J. Am. Chem. Soc.*, 2011, **133**, 2525-2534.
- 46 K. Sempf, T. Arrey, S. Gelperina, T. Schorge, B. Meyer, M. Karas and J. Kreuter, *Eur. J. Pharm. Biopharm.*, 2013, **85**, 53-60.
- 47 P. P. Karmali, Y. Chao, J. H. Park, M. J. Sailor, E. Ruoslahti, S. C. Esener and D. Simberg, *Mol. Pharm.*, 2012, **9**, 539-545.
- 48 O. Kassar, S. A. McMahan, R. Thompson, C. H. Botting, J. H. Naismith and A. J. Stewart, *Blood*, 2014, **123**, 1948-1955.
- 49 P. S. Nair and W. E. Robinson, *Arch. Biochem. Biophys.*, 1999, **366**, 8-14.
- 50 I. K. Poon, K. K. Patel, D. S. Davis, C. R. Parish and M. D. Hulett, *Blood*, 2011, **117**, 2093-2101.
- 51 D. B. Borza and W. T. Morgan, *J. Biol. Chem.*, 1998, **273**, 5493-5499.
- 52 A. L. Jones, M. D. Hulett and C. R. Parish, *Immunol. Cell Biol.*, 2005, **83**, 106-118.
- 53 V. Rydengard, A. K. Olsson, M. Morgelin and A. Schmidtchen, *FEBS J.*, 2007, **274**, 377-389.
- 54 V. Rydengard, O. Shannon, K. Lundqvist, L. Kacprzyk, A. Chalupka, A. K. Olsson, M. Morgelin, W. Jahnen-Dechent, M. Malmsten and A. Schmidtchen, *PLoS Pathog.*, 2008, **4**, e1000116.
- 55 O. Shannon, V. Rydengard, A. Schmidtchen, M. Morgelin, P. Alm, O. E. Sorensen and L. Bjorck, *Blood*, 2010, **116**, 2365-2372.
- 56 J. W. Bryant and Z. Shariat-Madar, *Cardiovasc. Hematol. Agents Med. Chem.*, 2009, **7**, 234-250.
- 57 R. Tavano, D. Segat, E. Reddi, J. Kos, M. Rojnik, P. Kocbek, S. Iratni, D. Scheglmann, M. Colucci, I. M. Echevarria, F. Selvestrel, F. Mancin and E. Papini, *Nanomedicine (Lond)*, 2010, **5**, 881-896.
- 58 N. Sheng, M. B. Fairbanks, R. L. Heinrichson, G. Canziani, I. M. Chaiken, D. M. Mosser, H. Zhang and R. W. Colman, *Blood*, 2000, **95**, 3788-3795.
- 59 S. K. Lee and J. L. Ding, *DNA Cell Biol.*, 2013, **32**, 36-40.
- 60 K. Poon, M. D. Hulett and C. R. Parish, *Blood*, 2010, **115**, 2473-2482.
- 61 K. K. Patel, I. K. Poon, G. H. Talbo, M. A. Perugini, N. L. Taylor, T. J. Ralph, N. J. Hoogenraad and M. D. Hulett, *IUBMB Life*, 2013, **65**, 550-563.
- 62 L. L. Leung, *J. Clin. Invest.*, 1986, **77**, 1305-1311.

- 63 C. Rolny, M. Mazzone, S. Tugues, D. Laoui, I. Johansson, C. Coulon, M. L. Squadrito, I. Segura, X. Li, E. Knevels, S. Costa, S. Vinckier, T. Dresselaer, P. Akerud, M. De Mol, H. Salomaki, M. Phillipson, S. Wyns, E. Larsson, I. Buysschaert, J. Botling, U. Himmelreich, J. A. Van Ginderachter, M. De Palma, M. Dewerchin, L. Claesson-Welsh and P. Carmeliet, *Cancer. Cell.*, 2011, **19**, 31-44.
- 64 S. Tugues, S. Honjo, C. Konig, O. Noguer, M. Hedlund, J. Botling, S. Deschoemaeker, M. Wenes, C. Rolny, W. Jahnen-Dechent, M. Mazzone and L. Claesson-Welsh, *Cancer Res.*, 2012, **72**, 1953-1963.
- 65 R. Tavano, S. Franzoso, P. Cecchini, E. Cartocci, F. Oriente, B. Arico and E. Papini, *J. Leukoc. Biol.*, 2009, **86**, 143-153.
- 66 J. L. Callum, K. Karkouti and Y. Lin, *Transfus. Med. Rev.*, 2009, **23**, 177-188.
- 67 A. L. Jones, I. K. Poon, M. D. Hulett and C. R. Parish, *J. Biol. Chem.*, 2005, **280**, 35733-35741.
- 68 D. B. Rylatt, D. Y. Sia, J. P. Mundy and C. R. Parish, *Eur. J. Biochem.*, 1981, **119**, 641-646.
- 69 M. M. Bradford, *Anal. Biochem.*, 1976, **72**, 248-254.